

Monodomain response of finite-aspect-ratio macromolecules in shear and related linear flows

M. Gregory Forest*, Qi Wang[†]

Abstract

Recent extensions of the Doi kinetic theory for monodisperse nematic liquids describe rigid, axisymmetric, ellipsoidal macromolecules with finite aspect ratio. Averaging and presumed linear flow fields provide tensor dynamical systems for mesoscopic, bulk orientation response, parametrized by molecular aspect ratio. In this paper we explore phenomena associated with finite versus infinite aspect ratios, which alter the most basic features of monodomain attractors: steady vs. unsteady, in-plane vs. out-of-plane, multiplicity of attracting states, and shear-induced transitions. For example, the Doi moment-closure model predicts a period-doubling cascade in simple shear to a chaotic monodomain attractor for aspect ratios nearby $3 : 1$ or $1 : 3$, similar to full kinetic simulations by Grosso et al. (2001) for infinite aspect ratios. We develop theoretical properties first, independent of closure approximation but specific to linear flow fields, which imply:

- the entire monodomain phase diagram of a finite-aspect-ratio nematic fluid in linear flow fields is equivalent to the phase diagram of an infinite-aspect-ratio fluid (thin rods or discs) with a related linear velocity field;
- rod-like and discotic macromolecules with reciprocal aspect ratios have equivalent bulk shear response, related by a simple director transformation;
- all shear-induced monodomains respect symmetries relative to the shearing plane, e.g., major director (kayaking) motions that rotate around an axis between the vorticity axis and shearing plane are always accompanied by a symmetric response reflected through the shear plane. This provides a symmetry mechanism for bi-stable attractors.

A tensor analog of the Leslie alignment vs. tumbling criterion is developed and applied. Simulations highlight the degree to which scaling properties of Leslie-Ericksen theory (e.g., shear response can be scaled in terms of strain units, monodomain transitions are independent of shear rate) are violated. With finite aspect ratios, any shear-induced monodomain is reproducible among the well-known closure approximations, yet no single closure rule suffices to capture all known attractors and transition scenarios.

*Department of Mathematics, University of North Carolina, Chapel Hill, Chapel Hill, NC 27599-3250

[†]Department of Mathematics, Florida State University, Tallahassee, FL 32306-4510

1 Introduction

Theoretical and numerical studies of homogeneous responses of nematic polymers and liquid crystals to simple shear have spanned four decades; a representative yet inexhaustive list is [35, 36, 56, 77, 5, 58, 116, 59, 27, 25, 57, 78, 119, 26, 30, 110, 20, 69, 70, 21, 111, 129, 86, 87, 72, 103, 109, 73, 81, 104, 79, 13, 39, 54, 55, 80, 82, 83, 4, 67, 23, 105, 117, 121, 120, 40, 112, 38, 52], contributing to a fundamental understanding of macromolecular fluids. These studies aspire to reproduce, explain, and predict experimental discoveries of monodomain behavior, e.g., [48, 96, 106, 65, 66, 113, 33, 107, 1, 50, 102, 97, 99, 18, 11, 19, 16, 114, 84, 32, 126, 6, 7, 53, 100, 125, 92, 34, 101, 93, 94, 95, 12, 15, 127]. Experimental imaging that allows comparison with theory has been enabled by advances in shear devices and rheo-optics, e.g., [11, 62, 47].

By a combination of theory and experiment, many steady and transient shear-induced, monodomain modes have been catalogued and *named primarily on the basis of director response*: steady alignment with primary director either in the shear plane (*flow aligning*) or along the vorticity axis (*logrolling*); in-plane transient oscillatory (*wagging*) or rotating (*tumbling*) director modes; and out-of-plane transient director modes (*kayaking*). Complicated dynamics is also possible. Recent full kinetic simulations of the Doi theory for monodomains [52] of infinite aspect ratio rigid rods indicate a shear window of highly erratic director motions, i.e., homogeneous director chaos, in contrast with the heterogeneous director turbulence noted earlier (e.g., [85]). In essence, monodomain behavior is the zero wave-vector subspace of the far more complex (and infinite dimensional) phenomena associated with spatial heterogeneity. Nonetheless, this finite-dimensional subspace is where the dynamics begins; monodomains play the important role of precursors to structure formation.

In our studies below, we pay particular attention to dynamics of the *degrees of orientation that accompany director motions*. The latter feature of mesoscopic tensor theories [57, 30, 31, 9] addresses behavior that is not captured from traditional L-E models, discussed below. As theory and simulation become more resolved, a clarification of the *a priori* consequences of a restricted, single-director theory seems prudent.

The characterization of monodomain shear response and all shear-rate-dependent transitions is routinely utilized, for example:

- for fundamental rheological classification of given nematic polymers [27] (e.g., "flow-aligning 5CB" [93] versus "tumbling 8CB" [94]);
- transitions between monodomain attractors (e.g., the tumbling to flow-aligning transition) correlate with measurable sign changes in first and second normal stress differences [65, 66, 110, 69, 70, 86, 87, 79, 72]; and

- as a precursor and indicator of subsequent formation of spatial structures and textures [19, 11, 114].

We refer to two important review papers by Marrucci and Greco [91] and Burghardt [17] for discussions of the rheological responses of sheared nematic polymers, and in particular the correlations between texture formation and monodomain modes for several different (flow-aligning versus tumbling) nematic fluids.

Below we will focus on transition phenomena in several tensor models; the effect of finite molecular aspect ratio will appear prominently. In a subsequent study, we follow many investigations into structure formation in processing-type flows which are well-approximated by linear flow fields. One of our motivations here is to have tensor models with sufficient flexibility to be able to characterize bulk monodomain response for a laboratory nematic liquid. The role of finite aspect ratio is shown in this paper to enrich the flow-phase diagrams of infinite-aspect-ratio tensor models, thereby capable of accomodating more complex monodomain behavior.

It is standard protocol to infer tumbling versus non-tumbling nematics *from the laboratory* by the structure of normal stress differences and apparent viscosity versus shear rate, clarified and developed in various laboratories ([102, 50, 98, 10, 71, 99, 51, 84, 114, 19, 74, 115, 75, 62, 61, 125, 17, 128, 15, 127]). Many experimental studies now routinely include model simulations, still dominated by Leslie-Ericksen theory. Likewise, it is *required protocol for theorists* to identify shear-driven phase transitions, and to classify the precise nature of those transitions so they may be confirmed or not by experiment. The explicit characterization of phase transitions in terms of bifurcation type has its roots in the work of Hess [57], Semenov [110], Kuzuu and Doi [69, 70], Marrucci and Maffettone [86], and Larson [72], and now has become a routine tool with application of modern software packages for identifying and classifying bifurcations (e.g., [13, 39, 54, 55, 80, 83, 108, 2, 3, 122, 112, 43, 45, 24]). Bifurcation analysis can illuminate qualitative features of monodomains at shear rates just below or above phase transitions. E.g., the classical Hopf bifurcation indicates loss or gain of a periodic degree of freedom [112]. We are interested in which orientation features (in-plane vs. out-of-plane components, directors vs. degrees of orientation) inherit the dynamics associated with bifurcations. Notably, we find a cascade of period doubling bifurcations to chaotic motion for the Doi closure model, strongly reminiscent of highly resolved full kinetic simulations by Grosso et al. [52]. We further refer the reader to mathematical treatments [49, 24] which apply equivariant bifurcation theory that deduce and construct heterogeneous patterns (some derived by alternative methods [44, 46]) based on symmetries of tensor equations; these powerful tools have only started to be applied toward nematic structure properties, where a host of space-time bifurcation phenomena await discovery.

The question of bifurcation type, and what bifurcations are possible, amplifies the issue of two-dimensional (director) versus five-dimensional (tensor) models for monodomains. *Two-dimensional autonomous dynamical systems cannot produce the complex dynamics revealed here.* Some critical *a priori* differences are:

- L-E theory *guarantees* a scaling property that allows superposition of data for any constant shear rate into a master curve in units of strain [77, 78, 91, 17, 127]. Small molecule liquid crystals appear to accurately obey this scaling law (e.g., [118]), as well as recent data [127] for in-plane shear alignment of certain main-chain thermotropes.
- The Doi [31], Landau-deGennes [27], or Beris-Edwards [9] mesoscopic tensor theories do not share this scaling property, as detailed below, essentially because of order parameter variation induced by the short-range, excluded-volume potential.
- There are no shear-rate-dependent monodomain transitions in L-E models, only viscosity-dependent transitions! Yet the tumbling-to-alignment transition is observed in tumbling nematics at a critical shear rate. By contrast, the full tensor theory admits a diversity of bifurcations versus shear rate for a fixed nematic liquid; moreover, these transitions dominate the weak flow regime for finite aspect ratios.

The current paper tests predictions of the recent Doi-type kinetic model of Wang [123], applied to shear-induced bulk behavior of finite-aspect-ratio, monodisperse, nematic liquids. We first summarize the modern Doi kinetic theory and the mesoscopic orientation tensor model that follows, prior to closure approximation. Four popular closure rules are then recalled. Our new results begin with symmetry properties of the mesoscopic theory that are independent of closure approximation, together with experimental implications of these symmetry properties. We then develop a tensor version of a Leslie alignment-versus-tumbling criterion, and study the selection mechanism of steady and periodic monodomains in the weak shear limit. This explains the multiplicity and stability of monodomain solutions in the weak shear limit, and the remarkable sensitivity of selection criteria both on closure rule and molecular aspect ratio. It is then possible to use continuation software packages to follow the solution branches versus shear rate for a given aspect ratio and closure rule. After recalling infinite aspect ratio results, we focus on behavior associated with a finite molecular aspect ratio in the range 3 : 1 to 20 : 1, for rod-like (prolate) or disc-like (oblate) axisymmetric ellipsoidal molecules. We then proceed to the primary quantitative results of each closure model, i.e., detailed flow-phase bifurcation diagrams. The dramatic role of aspect ratio is illustrated in various ways.

2 Kinetic theory and mesoscopic models for finite-aspect-ratio nematic fluids

We briefly review the homogeneous form of the Doi-type kinetic model of Wang [123] only to the extent necessary to reproduce results of this paper. We assume nematic polymer liquids consisting of monodisperse, rigid, axisymmetric ellipsoidal molecules immersed in a viscous solvent. The molecules are characterized by an axis of symmetry, \mathbf{m} , and an aspect ratio r of the length along the symmetry axis divided by the radius of the transverse circular cross-section. Infinitely thin rods, spheres, and infinitely thin discs correspond to $r = \infty, 1, 0$, respectively. This kinetic model shares features with several other models (e.g., [69, 70, 117, 41, 68]), including molecular geometry, orientation-dependent rotary diffusivity, excluded-volume effects, and distortional elasticity potentials of Marrucci and Greco [89, 90, 91]. The latter effects do not come into play for monodomain dynamics addressed here, but are essential for subsequent morphology formation; e.g., the highly disparate elasticity constants for rod-like vs. discotic nematics does not enter here. Once the kinetic model is summarized, we discuss four closure approximations that yield simplified approximate models.

Let $f(\mathbf{m}, \mathbf{x}, t)$ be the distribution function corresponding to the probability that the axis of revolution of the molecule is parallel to direction \mathbf{m} ($\|\mathbf{m}\| = 1$) at location \mathbf{x} and time t . The fluid velocity is denoted \mathbf{v} . The Smoluchowski (kinetic) equation for $f(\mathbf{m}, \mathbf{x}, t)$, neglecting translational diffusion as is customary, is given by (e.g., [31, 14, 27]):

$$\frac{Df}{Dt} = \mathcal{R} \cdot [D_r(\mathbf{m}, a)(\mathcal{R}f + \frac{1}{kT}f\mathcal{R}V_{MS})] - \mathcal{R} \cdot [\mathbf{m} \times \dot{\mathbf{m}}f], \quad (1)$$

where $\frac{D}{Dt}(\bullet)$ denotes the material derivative $\frac{\partial}{\partial t}(\bullet) + \mathbf{v} \cdot \nabla(\bullet)$, $\frac{\partial}{\partial \mathbf{x}} = \nabla$ and $\mathcal{R} = \mathbf{m} \times \frac{\partial}{\partial \mathbf{m}}$ are the spatial and the rotational gradient operator, respectively;

$$\dot{\mathbf{m}} = \boldsymbol{\Omega} \cdot \mathbf{m} + a[\mathbf{D} \cdot \mathbf{m} - \mathbf{D} : \mathbf{m}\mathbf{m}\mathbf{m}] \quad (2)$$

is the Jeffrey orbit of ellipsoids [63], \mathbf{D} and $\boldsymbol{\Omega}$ are the rate of strain and vorticity tensors, defined by (with the convention $(\nabla \mathbf{v})_{ij} = \frac{\partial v_i}{\partial x_j}$)

$$\mathbf{D} = \frac{1}{2}(\nabla \mathbf{v} + \nabla \mathbf{v}^T), \quad \boldsymbol{\Omega} = \frac{1}{2}(\nabla \mathbf{v} - \nabla \mathbf{v}^T), \quad (3)$$

$-1 \leq a \leq 1$ is the *molecular shape parameter* related to the molecular aspect ratio r by

$$a = \frac{r^2 - 1}{r^2 + 1}. \quad (4)$$

Note that $a \approx 1$ corresponds to the thin rod limit; $a = 0$ corresponds to spherical molecules; and $a \approx -1$ corresponds to the thin disc limit. The rotary diffusion coefficient in (1) is defined by

$$D_r(\mathbf{m}, a) = \hat{D}_r(a) \left(\int_{\|\mathbf{m}'\|=1} \|\mathbf{m} \times \mathbf{m}'\| f(\mathbf{m}', \mathbf{x}, t) d\mathbf{m}' \right)^{-2}, \quad (5)$$

where the pre-factor $\hat{D}_r(a)$ is a (possibly aspect-ratio-dependent) *rotary diffusion constant*, k is the Boltzmann constant, T is the absolute temperature, and V_{MS} is the Maier-Saupe intermolecular potential with strength proportional to the *dimensionless polymer concentration* N :

$$V_{MS} = -\frac{3NkT}{2} \langle \mathbf{m}\mathbf{m} \rangle : \mathbf{m}\mathbf{m}. \quad (6)$$

Averaged mesoscopic orientation of the nematic molecules \mathbf{m} is captured by

$$\mathbf{M} = \langle \mathbf{m}\mathbf{m} \rangle = \int_{\|\mathbf{m}\|=1} \mathbf{m}\mathbf{m} f(\mathbf{m}, \mathbf{x}, t) d\mathbf{m}, \quad (7)$$

the second moment of \mathbf{m} with respect to the probability density function (pdf). Traditionally, one normalizes \mathbf{M} to have zero trace, and

$$\mathbf{Q} = \langle \mathbf{m}\mathbf{m} \rangle - \frac{\mathbf{I}}{3} \quad (8)$$

is called the **orientation tensor**. \mathbf{M} and \mathbf{Q} share an orthonormal frame of eigenvectors, called the **directors** or optical axes, with corresponding eigenvalues $d_i, i = 1, 2, 3$ of \mathbf{M} , $d_i - \frac{1}{3}$ of \mathbf{Q} , called the **order parameters** where

$$\begin{aligned} d_i &= \langle (\mathbf{m} \cdot \mathbf{n}_i)^2 \rangle, \\ d_1 + d_2 + d_3 &= 1, \end{aligned} \quad (9)$$

$$\mathbf{Q} = \sum_{i=1}^3 (d_i - \frac{1}{3}) \mathbf{n}_i \mathbf{n}_i.$$

Each $0 \leq d_i \leq 1$ conveys the degree to which the mesoscale ensemble of molecules \mathbf{m} is aligned with respect to the primary directors \mathbf{n}_i . Geometrically \mathbf{M} or \mathbf{Q} uniquely define an **orientation ellipsoid** whose semi-axes are prescribed by the directors \mathbf{n}_i and whose axes lengths are the respective degrees of orientation d_i . Furthermore, spatial homogeneity grants that we can completely specify all monodomain solutions by steady or time-lapse visualization of the ellipsoids relative to the shear flow and flow gradient directions. This imaging of monodomains has been utilized by many authors; we refer to the review by Marrucci and Greco [91] for a compelling discussion. The reader may refer forward to Figures 3, 4, 5 for the mesoscale ellipsoids associated with $\mathbf{Q}(t)$. We further extract from the ellipsoid the director motion on the sphere (the major director alone would be akin to

a L-E simulation) [112], and the order parameter motion (which measures departure from L-E theory). Similar to the L-E continuum theory, the second-moment tensor mimics the molecular geometry at the mesoscopic scale: the axisymmetric ellipsoidal molecule becomes (upon averaging) a full ellipsoid with three distinct semi-axes lengths d_i .

The maximum normalized birefringence is the maximum of $|d_i - d_j|$, occurring in the plane of $\mathbf{n}_i, \mathbf{n}_j$. The nematic is: *biaxial* if the d_i are distinct; *uniaxial* if $d_i = d_j \neq d_k$, in which case the director \mathbf{n}_k of the simple eigenvalue is “the” director; and *isotropic* if all $d_i = \frac{1}{3}$, i.e., $\mathbf{Q} = \mathbf{0}$. The *major director* is defined as \mathbf{n}_k for which $|d_k - \frac{1}{3}|$ is the unique maximum, indicating the largest departure from random molecular alignment along the major director. By comparison, the Leslie-Ericksen continuum theory corresponds to two restrictions on the tensor \mathbf{Q} : uniaxiality (i.e., a unique director), and the molecule axis is identical with the director. These translate to fixing the d_i at values 1,0,0 which removes two degrees of freedom, and losing one director degree of freedom in the isotropic plane transverse to the director.

A dynamical equation for the orientation tensor \mathbf{Q} is derived by taking the second moment of \mathbf{m} with respect to the pdf, then using the kinetic equation (1) and Jeffrey molecule dynamics (2):

$$\begin{cases} \frac{D}{Dt}\mathbf{Q} - \Omega \cdot \mathbf{Q} + \mathbf{Q} \cdot \Omega - a[\mathbf{D} \cdot \mathbf{Q} + \mathbf{Q} \cdot \mathbf{D}] = \frac{2a}{3}\mathbf{D} - 2a\mathbf{D} : \langle \mathbf{m}\mathbf{m}\mathbf{m}\mathbf{m} \rangle \\ -6D_r^0[\mathbf{Q} - N(\mathbf{Q} + \frac{\mathbf{I}}{3}) \cdot \mathbf{Q} + N\mathbf{Q} : \langle \mathbf{m}\mathbf{m}\mathbf{m}\mathbf{m} \rangle], \end{cases} \quad (10)$$

where

$$D_r^0 = \begin{cases} \frac{\tilde{D}_r^0}{(1 - \frac{3}{2}\mathbf{Q}:\mathbf{Q})^2}, & \text{with orientation-dependent rotary diffusivity,} \\ \tilde{D}_r^0, & \text{without orientation-dependent rotary diffusivity,} \end{cases} \quad (11)$$

\tilde{D}_r^0 is a constant averaged rotary diffusivity that results from the averaging process [31].

For future purposes of monitoring the first and second normal stress differences, we record the homogeneous stress tensor (apart from an isotropic pressure):

$$\begin{aligned} \tau = & (2\eta + 3ckT\zeta_3(a))\mathbf{D} + 3a\nu kT[\mathbf{Q} - N(\mathbf{Q} + \frac{\mathbf{I}}{3})\mathbf{Q} + N\mathbf{Q} : \langle \mathbf{m}\mathbf{m}\mathbf{m}\mathbf{m} \rangle] \\ & + 3\nu kT[\zeta_1(a)(\mathbf{D}\mathbf{M} + \mathbf{M}\mathbf{D}) + \zeta_2(a)\mathbf{D} : \langle \mathbf{m}\mathbf{m}\mathbf{m}\mathbf{m} \rangle], \end{aligned} \quad (12)$$

where η is the solvent viscosity, $\zeta_{1,2,3}(a)$ are three shape-dependent friction coefficients given in the Appendix, and ν is the number density of LCP molecules per unit volume.

These equations, coupled with momentum, mass and energy balance equations, constitute the modified Doi equations for nematic polymer fluids. For *isothermal, linear flow fields*, these conservation laws are satisfied identically, and the full system “simplifies” to

the homogeneous orientation tensor dynamics governed by (10). However, the presence of fourth-order tensors in (10) and the extra stress (12) couples the second-moment evolution equation to fourth-moments, requiring one either to continue to generate higher moment equations and truncate at some finite order, or to solve the Smoluchowski equation (1) directly, as in [73, 80, 83, 38, 52]. To avoid this computational and analytical complexity, many authors have introduced closure approximations, a tack which we follow in this paper. Note that one needs only to approximate products of $\langle \mathbf{m m m m} \rangle$ with various second order tensors. We now recall four well-known closure approximations that have been effective in specific applications:

Quadratic (Doi) closure

$$(\bullet) : \langle \mathbf{m m m m} \rangle \approx (\bullet) : \mathbf{M M}, \quad (13)$$

where (\bullet) is any second order tensor.

Rey-Tsuji (RT) closure

Rey and Tsuji [117] employed the rule:

$$\begin{aligned} (\bullet) : \langle \mathbf{m m m m} \rangle \approx & \frac{1}{4}[(\bullet) : \mathbf{Q Q} + (\bullet) \mathbf{Q}^2 + \mathbf{Q}(\bullet) \mathbf{Q} + \mathbf{Q}^2(\bullet) \\ & - ((\bullet) \mathbf{Q}) : \mathbf{Q I}] + \frac{1}{3}((\bullet) : \mathbf{Q}) \mathbf{I}. \end{aligned} \quad (14)$$

Hinch and Leal developed two closure approximations in their studies of suspension rheology [60].

Hinch-Leal 1 (HL1) closure

$$\begin{aligned} (\bullet) : \langle \mathbf{m m m m} \rangle \approx & \frac{1}{5}[6 \mathbf{M}(\bullet) \mathbf{M} - \mathbf{M M} : (\bullet) - \\ & 2(\mathbf{M M}) : (\bullet) \mathbf{I} + 2 \mathbf{M} : (\bullet) \mathbf{I}]. \end{aligned} \quad (15)$$

Hinch-Leal 2 (HL2) closure

$$\begin{aligned} (\bullet) : \langle \mathbf{m m m m} \rangle \approx & \mathbf{M}(\mathbf{M} : (\bullet)) + 2[\mathbf{M}(\bullet) \\ & \mathbf{M} - (\mathbf{M})^2(\mathbf{M}^2 : (\bullet))/(\mathbf{I} : (\mathbf{M}^2))] + \\ & \alpha(\mathbf{M})[\frac{52}{315}(\bullet) - \frac{8}{21}[(\bullet) \mathbf{M} + \mathbf{M}(\bullet) - \frac{2}{3}(\mathbf{M} : (\bullet)) \mathbf{I}]], \end{aligned} \quad (16)$$

where

$$\alpha(\mathbf{M}) = \exp[2(\mathbf{I} - 3 \mathbf{M}^2 : \mathbf{I})/(\mathbf{I} - \mathbf{M}^2 : \mathbf{I})]. \quad (17)$$

These closure approximations have been used in the Doi theory *with infinite molecular aspect ratio* ($|a| = 1$) in both simple shear [73, 23, 117, 121] and extensional flows [122, 108, 43, 45] and even more complex geometries [40]. A general conclusion would be that there is no clear best closure for all flows and flow rates. For example, the quadratic closure gives reasonable predictions in strong (elongational) flows [122, 108, 43, 46] and flows with a slight stretching [23]; the HL-2 closure is superior with respect to the tumbling parameter versus equilibrium order parameter comparisons with the full kinetic theory [60, 72]. To our knowledge, no systematic evaluation of closure rules has been performed for shear-driven flows of finite-aspect-ratio macromolecules. Such a study seems especially warranted due to the significant qualitative changes in each closure model induced by finite versus infinite molecular geometry. Singh and Rey [112] compared closures at the finite discotic ratio $r = \frac{1}{3}$.

These closure rules may each be applied with constant rotary diffusivity (21b) and with orientation-dependent rotary diffusivity (21a). The following prescriptions have been used in the references above, providing the model systems we now analyze:

Modified Doi Model: the quadratic closure is applied everywhere for $(\bullet) : \langle \mathbf{m m m m} \rangle$.

Doi-Rey-Tsuji Model: the quadratic closure is applied to $\mathbf{M} : \langle \mathbf{m m m m} \rangle$ in the orientation tensor equation, and the Rey-Tsuji closure is used for all other terms.

Modified Doi-Hinch-Leal Models: the quadratic closure is applied to $\mathbf{M} : \langle \mathbf{m m m m} \rangle$ in the orientation tensor equation, and the H-L1 or H-L2 closure is applied for all other fourth-order moment terms.

3 Monodomain responses to linear flows with a shear component

We begin by noting two important correspondences that follow from the Doi mesoscopic theory: one between finite and infinite aspect-ratio nematic fluids in related linear flow fields, and the other between rod-like and discotic molecules in the same linear flow field. These properties are *independent of closure approximation*, and therefore follow for all of the models we analyze in the next two sections.

We are primarily concerned with simple steady shear flow in Cartesian coordinates (x, y, z) with constant shear rate $\dot{\gamma}$:

$$\mathbf{v}_{shear} = \dot{\gamma}(y, 0, 0). \tag{18}$$

The *shear timescale* $t_s = \dot{\gamma}^{-1}$ competes with the average *nematic relaxation timescale*, $t_n = \frac{1}{6D_r^0}$, which we presume to be fixed for a given nematic fluid. We nondimensionalize (10) in nematic relaxation time units:

$$\begin{aligned} \frac{\partial}{\partial \tilde{t}} \mathbf{Q} - Pe[\tilde{\mathbf{\Omega}} \cdot \mathbf{Q} - \mathbf{Q} \cdot \tilde{\mathbf{\Omega}} + a(\tilde{\mathbf{D}} \cdot \mathbf{Q} + \mathbf{Q} \cdot \tilde{\mathbf{D}})] &= aPe[\frac{2}{3}\tilde{\mathbf{D}} - 2\tilde{\mathbf{D}} : \langle \mathbf{m m m m} \rangle] \\ -\frac{1}{\Lambda}[\mathbf{Q} - N(\mathbf{Q} + \frac{1}{3}\mathbf{I}) \cdot \mathbf{Q} + N\mathbf{Q} : \langle \mathbf{m m m m} \rangle], \end{aligned} \quad (19)$$

where $\tilde{t} = \frac{t}{t_n}$, and the *Peclet number*

$$Pe = t_n \dot{\gamma} \quad (20)$$

is the shear rate normalized by the average rate of rotational diffusivity. (Note: this ratio also defines a Deborah number, e.g. [75, 17].) The dimensionless rotary diffusion is then

$$\Lambda = \begin{cases} (1 - \frac{3}{2}\mathbf{Q} : \mathbf{Q})^2, & \text{with orientation-dependent rotary diffusivity,} \\ 1, & \text{otherwise.} \end{cases} \quad (21)$$

The dimensionless rate-of-strain and vorticity tensors for simple shear flow (18) are

$$\tilde{\mathbf{D}}_{shear} = \frac{1}{2} \begin{pmatrix} 0 & 1 & 0 \\ 1 & 0 & 0 \\ 0 & 0 & 0 \end{pmatrix}, \quad \tilde{\mathbf{\Omega}}_{shear} = \frac{1}{2} \begin{pmatrix} 0 & 1 & 0 \\ -1 & 0 & 0 \\ 0 & 0 & 0 \end{pmatrix}. \quad (22)$$

3.1 A molecular geometry: straining flow scaling property

The equation (19) defines a “triple”: $(a, \tilde{\mathbf{v}}, \mathbf{Q})$, consisting of a nematic fluid of geometry parameter a and aspect ratio r ; any linear flow $\tilde{\mathbf{v}}$; and the corresponding monodomain orientation tensor \mathbf{Q} . An arbitrary *linear flow* in dimensionless form is given by

$$\tilde{\mathbf{v}} = (\tilde{\mathbf{\Omega}} + \tilde{\mathbf{D}})\tilde{\mathbf{x}}, \quad (23)$$

where $\tilde{\mathbf{D}}$ and $\tilde{\mathbf{\Omega}}$ are constant, and $trace(\tilde{\mathbf{D}}) = 0$.

We observe from (19) that the rate-of-strain tensor $\tilde{\mathbf{D}}$ and geometry parameter a enter linearly, and only through their product. This fact underlies two symmetries of the system (19) which we describe in terms of the triple defined above:

$$\begin{aligned} (a, \tilde{\mathbf{v}}, \mathbf{Q}) &\rightarrow (1, \tilde{\mathbf{v}} - (1 - a)\tilde{\mathbf{D}}\tilde{\mathbf{x}}, \mathbf{Q}), \\ (a, \tilde{\mathbf{v}}, \mathbf{Q}) &\rightarrow (-1, \tilde{\mathbf{v}} - (1 + a)\tilde{\mathbf{D}}\tilde{\mathbf{x}}, \mathbf{Q}). \end{aligned} \quad (24)$$

These symmetries imply an *identical monodomain response* \mathbf{Q} of: a finite aspect ratio fluid with geometry parameter a in any linear flow field, *and*, extremely thin rodlike *or*

discotic fluids, respectively, in a linear superposition of the identical linear flow field with a pure strain component of magnitude $1 - |a|$ or $1 + |a|$. This correspondence implies intriguing experimental advantages; we note two obvious examples here. Shear-induced (more generally, any linear flow-induced) monodomain behavior of *an entire spectrum of monodisperse nematic liquids* can be inferred from flow experiments on *a single large-aspect-ratio nematic liquid* by controlling the amplitude of the straining component while holding the vorticity component fixed. Alternatively, one can use a simple shear device with a finite-aspect-ratio, monodisperse nematic liquid, to mimic more general linear flows of large aspect ratio macromolecular fluids.

This correspondence indicates why a simple change in aspect ratio could lead, especially in the weak flow limit, to dramatic changes in monodomain response. Experiments would be valuable to test the validity of the general mesoscopic model (19). *We emphasize that these properties are restricted to linear flows and homogeneous orientation behavior.*

3.2 A rodlike-discotic correspondence in simple shear

The mesoscale model (19), again independent of any approximations used for the fourth-order moment in this paper, admits a special symmetry specific to a fixed shear flow (18,22):

$$(a, \tilde{\mathbf{v}}_{shear}, \mathbf{Q}) \rightarrow (-a, \tilde{\mathbf{v}}_{shear}, \mathbf{V}_1^t \mathbf{Q} \mathbf{V}_1), \quad (25)$$

where

$$\mathbf{V}_1 = \begin{pmatrix} 0 & 1 & 0 \\ -1 & 0 & 0 \\ 0 & 0 & 1 \end{pmatrix}. \quad (26)$$

\mathbf{V}_1 is an orthogonal matrix corresponding to a 90° rotation in the $x - y$ (shearing) plane, while holding the vorticity axis fixed. Recall a and $-a$ correspond to reciprocal aspect ratios, r and r^{-1} . Also recall that similarity transform by an orthogonal matrix leaves the order parameters (eigenvalues) invariant, while rotating the orthonormal frame of directors (eigenvectors) in the shear plane. This symmetry implies: *for any pure shear flow, the monodomain response of discotic polymers with monodisperse aspect ratio $r < 1$ is identical to that of rod-like polymers with aspect ratio r^{-1} , where the mesoscopic directors are related by a simple 90° rotation in the shearing plane.*

We note that the symmetry (26) maps either of the two symmetries (24) to the other in simple shear flows. This correspondence in its simplest form (flow-aligning steady states) is obvious: if the major director of rod-like molecules aligns in the flow direction, then discotic molecules of the reciprocal aspect ratio will, on average, align in the flow gradient direction.

However, it generalizes to arbitrary monodomain response, e.g., phase transitions and all stable and unstable monodomains occur simultaneously for rods and discs of reciprocal aspect ratios. (An analogous correspondence exists for purely extensional flows [45], which was used to infer extensional orientation steady states of discotic LCs from the results in [43] for rod-like LCs.) *We caution that the constitutive stress equation does not have this symmetry, so that the correspondence will break down with spatial structure.*

4 Analysis of the Doi monodomain model with simple shear

We now focus on the Doi mesoscopic model (19) with imposed pure shear flows (18), (22). Following the historical literature, one is interested in all stable or attracting states $\mathbf{Q}(t)$, steady or transient, at each fixed shear rate. Two theoretical results are presented here which directly impact *multiplicity* and *alignment criteria* for attracting states, independent of closure approximation and for any aspect ratio fluid.

4.1 Out-of-plane monodomain modes come in pairs

The Doi mesoscopic orientation equation (19), for all the closure approximations employed in this paper and with a presumed pure shear flow and molecular aspect ratio r , admits a reflection symmetry:

$$(a, \tilde{\mathbf{v}}_{shear}, \mathbf{Q}) \rightarrow (a, \tilde{\mathbf{v}}_{shear}, \mathbf{V}_2^t \mathbf{Q} \mathbf{V}_2), \quad (27)$$

where

$$\mathbf{V}_2 = \begin{pmatrix} 1 & 0 & 0 \\ 0 & 1 & 0 \\ 0 & 0 & -1 \end{pmatrix}. \quad (28)$$

Similarity transform of \mathbf{Q} by \mathbf{V}_2 corresponds to:

- an identity transformation for in-plane modes, i.e., solutions satisfying $(Q_{xz}, Q_{yz}) = (0, 0)$; yet,
- a discrete reflection symmetry among out-of-plane monodomain states: any solution \mathbf{Q} with non-zero out-of-plane components (Q_{xz}, Q_{yz}) generates another solution with identical in-plane components but out-of-plane components $(-Q_{xz}, -Q_{yz})$.

This symmetry is natural: nothing in the experiment as modeled, or the equations, selects the direction of tilt out-of-plane. Yet there are intriguing consequences of this symmetry for so long as the orientation response is homogeneous. We mention some:

- In-plane data remains in-plane unless given an out-of-plane perturbation. In all models and parameter regimes, in-plane solutions exist which require careful stability analysis to out-of-plane perturbations.
- Out-of-plane orientation data cannot become in-plane in finite time, and *no monodomain motion can pass through the shearing plane*. E.g., out-of-plane oscillatory attractors whose major director has escaped the shearing plane at some critical shear rate stay tilted to one side of the shearing plane! Experimentally, this means one will see major director motion either on one side of the shearing plane or the other in a given realization. Indeed, if the shearing plane is crossed, it must be associated with heterogeneity.
- Out-of-plane monodomain solutions generate a mirror-symmetric monodomain, tilted strictly to the other side of the shearing plane:
 - if the major director either aligns with the vorticity axis (the logrolling state) or rotates around the vorticity axis (the kayaking orbit of Larson and Ottinger which we label \mathbf{K}_1 below), then this symmetry is an identity transformation;
 - if the major director lies between the vorticity axis and shearing plane (the solutions labeled \mathbf{K}_2 below), the monodomains occur in distinct pairs, each tilted exclusively to one side of the shearing plane.

(We defer further mathematical details to another treatment, such as infinite-time orbits, domains of attraction when there are multiple attractors, and linearized decay rates for periodic attractors. These issues are relevant to experimental studies, cf. van Horn and Winter [118] on the transient approach to stable monodomains.)

4.2 \mathbf{Q} tensor representations

We now introduce representations of \mathbf{Q} that allow us to amplify director and order parameter properties of monodomains, to visualize both steady and transient monodomain solutions, and to easily identify in-plane from out-of-plane monodomain states.

The representation (9) of \mathbf{Q} has an equivalent form (using the identity of directors $\sum \mathbf{n}_i \mathbf{n}_i = \mathbf{I}$),

$$\mathbf{Q} = s(\mathbf{n}_1 \mathbf{n}_1 - \frac{\mathbf{I}}{3}) + \beta(\mathbf{n}_2 \mathbf{n}_2 - \frac{\mathbf{I}}{3}), \quad (29)$$

where s and β arise from a simple linear transform of d_i to detect birefringence in each plane of the directors \mathbf{n}_i :

$$\begin{aligned} s &= \langle (\mathbf{m} \cdot \mathbf{n}_1)^2 \rangle - \langle (\mathbf{m} \cdot \mathbf{n}_3)^2 \rangle = d_1 - d_3, \\ \beta &= \langle (\mathbf{m} \cdot \mathbf{n}_2)^2 \rangle - \langle (\mathbf{m} \cdot \mathbf{n}_3)^2 \rangle = d_2 - d_3. \end{aligned} \tag{30}$$

The eigenvalue inequalities $|d_i| \leq 1$ confine the pair (s, β) to a triangular domain depicted in Figure 2. Note that isotropy in the plane of $\mathbf{n}_{1,3}, \mathbf{n}_{2,3}, \mathbf{n}_{1,2}$ is given by the respective conditions $s = 0, \beta = 0, s = \beta$, corresponding to the vertical, horizontal, and diagonal axes of Figure 2. Thus from Column 3 of Figures 3, 4, and 5 one can easily monitor the degree of biaxiality during all monodomain motions by noting distance from these uniaxial axes.

From (29), in-plane orientation is characterized by confinement of the directors $\mathbf{n}_1, \mathbf{n}_2$ to the shearing plane (x, y) , with \mathbf{n}_3 along the vorticity (z) axis. Recall $Q_{xz} = Q_{yz} = 0$ iff the orientation tensor is in-plane, giving easy recognition of in-plane versus out-of-plane solutions either by monitoring these entries or by visualizing the directors relative to the shearing plane.

4.3 Tensorial analog of the Leslie director alignment criterion

Classical studies of Jeffrey [63], Ericksen [35, 36], Leslie [77], Jenkins [64], Hinch-Leal [60], Larson [72], and many others in the past decade have aimed toward criteria for steady versus unsteady motion of liquid crystals and nematic polymers. We refer to two recent articles [118, 127] where L-E theory is applied to model dynamic and steady alignment data [15]. As emphasized in the review article of Marrucci and Greco [91], *a critical consequence of L-E theory is the existence of a scaling law*: monodomain response to simple shear depends on shear rate only through the product $\dot{\gamma}t$, and therefore all experimental data may be superposed in units of strain [127].

From a dynamical systems perspective, *the scaling law follows from two properties of the L-E director equations*:

- the equations are autonomous for simple shear with constant shear rate, and
- the shear rate enters only as a constant factor multiplying each director equation.

The Doi mesoscopic model preserves the first but patently violates the second property! It is precisely the intermolecular potential terms in (19), proportional to Λ^{-1} , that do not allow a re-scaling of time to absorb the normalized shear rate (Pe). The bottom line is that *solutions of the Doi tensor equation (19) cannot be scaled in terms of strain units*. Nontrivial

order parameter dynamics accompany the director motion, which is dominated by the shear-rate-dependent terms in (19). In a special limit of weak flow and near-equilibrium uniaxial nematic ordering, such as $0 \approx \Lambda^{-1} \ll Pe \ll 1$, the Doi monodomain tensor equation (19) can be cast in the L-E limit. Rather than carry out such a complicated asymptotic limit whose accuracy and experimental relevance is difficult to control, we choose to study the full tensor system and *a posteriori* monitor flow regimes and molecular aspect ratios where a L-E scaling law is approximately observed, or not.

We now derive an analogue of the Leslie selection criterion from which alignment versus unsteady transitions are rigorously characterized in mesoscopic tensor models. We give details for the Modified Doi Model; the other models are more tedious but the same analysis applies. This analysis extends in-plane criteria from [121] to finite aspect ratios, which we now show has a significant impact.

Consider “in-plane” motions with \mathbf{n}_1 and \mathbf{n}_2 confined to the shear plane $((x, y))$, admitting a single in-plane director angle ξ ,

$$\mathbf{n}_1 = (\cos \xi, \sin \xi, 0), \mathbf{n}_2 = (-\sin \xi, \cos \xi, 0). \quad (31)$$

The Modified Doi Model derived from (19) reduces from five coupled scalar equations to a system of three equations for (s, β, ξ) :

$$\begin{aligned} \frac{\partial s}{\partial t} &= -\frac{1}{\Lambda(s, \beta)} [U(s) - \frac{2N\beta s}{3}(s - \beta - 1)] + \frac{aPe}{3}(1 - \beta + 2s + 3\beta s - 3s^2) \sin 2\xi, \\ \frac{\partial \beta}{\partial t} &= -\frac{1}{\Lambda(s, \beta)} [U(\beta) - \frac{2N\beta s}{3}(\beta - s - 1)] - \frac{aPe}{3}(1 + 2\beta - s + 3\beta s - 3\beta^2) \sin 2\xi, \\ \frac{\partial \xi}{\partial t} &= \frac{Pe}{6(s-\beta)} [-3(s - \beta) + a(2 + \beta + s) \cos 2\xi], \end{aligned} \quad (32)$$

where $\int U(s)ds$ is the uniaxial bulk free energy potential function with

$$U(s) = s(1 - \frac{N}{3}(1 - s)(2s + 1)), \quad (33)$$

and

$$\Lambda(s, \beta) = \begin{cases} \frac{1}{(1 - (s^2 + s\beta + \beta^2))^2}, & \text{with orientation-dependent rotary diffusivity,} \\ 1, & \text{otherwise.} \end{cases} \quad (34)$$

The right-hand-side of (32.c) is recognized as a shear-imposed torque on the in-plane directors $\mathbf{n}_{1,2}$, completely analogous to the torque balance derived from a Leslie-Ericksen theory [36, 77, 64, 72]. The term independent of the geometry parameter a is a constant torque from the vorticity tensor, and the term proportional to a is the strain-induced torque which must be sufficiently strong to arrest tumbling. Steady flow-alignment requires this

torque balance to vanish, which yields a

Doi orientation tensor version of the Leslie in-plane director alignment criterion:

$$\cos 2\xi = \frac{1}{a} \frac{3(s - \beta)}{2 + s + \beta} = \frac{1}{a} \frac{d_1 - d_2}{d_1 + d_2}. \quad (35)$$

When $|a| = 1$, the right-hand-side (RHS) of (35) is always confined between -1 and 1 for all (s, β) in the allowable triangular domain shown in Figure 2a. One then uses (35) to replace $\sin 2\xi$ in (32a,b), giving two polynomial equations that are then solved for all roots (s_*, β_*) within the allowable domain. Each such equilibrium pair automatically yields a *flow-aligned, in-plane steady state*: (s_*, β_*) fixes the degrees d_i of biaxial nematic order along respective optical axes \mathbf{n}_i ,

$$d_1 = \frac{1}{3}(2s_* - \beta_* + 1), d_2 = \frac{1}{3}(2\beta_* - s_* + 1), d_3 = \frac{1}{3}(1 - s_* - \beta_*), \quad (36)$$

each pair (s_*, β_*) inserted into (35) prescribes exactly *two in-plane director alignment angles* $\xi \pmod{\pi}$, with \mathbf{n}_3 parallel to the vorticity axis. (A different representation is required to capture alignment out of the shear plane; we omit the details.)

When $|a| < 1$, however, the RHS of (35) exceeds 1 in absolute value over a subset of the allowable triangular domain of (s, β) , shown in Figure 2 for different values of a for the analogous director angle condition corresponding to each closure rule. In every closure model, the steady region diminishes as $|a|$ decreases, i.e., as the aspect ratio r approaches 1; *in the spherical molecule limit* $a = 0$, *the straining torque vanishes and no molecular alignment is possible*, consistent with known observation. We label the subset of the triangle where $|RHS| > 1$ as **U** (for unsteady), and the triangle subset where $RHS \leq 1$ as **S** (for steady). Note the regions **S**, **U** are *independent of the rotary diffusivity form* in (21). The zeros of (32a,b) for $|a| = 1$ (and the analogous calculation for the other seven models) are then monitored as $|a|$ decreases, with the following possible scenarios:

- equilibria reside within set **S**, providing a steady alignment angle ξ for each discrete solution of (35) or the analogous out-of-plane equation;
- equilibria move into set **U**, the in-plane (or out-of-plane) directors cannot flow-align, yielding transition to unsteady motion.

(The stability of these shear-selected steady equilibria, and the type and stability of unsteady states, are addressed below.)

From Figure 2a, the unsteady regions of the triangle grow from an empty set for the Modified Doi Model with $|a| = 1$ to consume the entire triangle in the limit of spherical molecules. Figures 2b,c,d show the analogous unsteady regions for the other closure models,

which have unsteady regions even for $|a| = 1$ corresponding to time-periodic solutions noted previously in the literature [73, 121, 23]. The analogous in-plane equations corresponding to (32) for the other closures are easily deduced by applying the same \mathbf{Q} representation to the respective tensor equations; the equations are omitted but results summarized next for all models.

It is thus clear, no matter what closure is used, that finite-aspect-ratio monodisperse solutions may experience unsteady responses where an infinitely thin rod or platelet is predicted to have shear-aligned steady monodomains. Further details of the selection mechanism are detailed next for each closure.

4.4 Multiplicity of monodomains: the weak shear limit $Pe \approx 0$

The development of rigorous criteria and theory for the selection of monodomain solutions in the limit $Pe \approx 0$ is nontrivial and still an open mathematical problem; we refer to Marrucci and Greco [91] for an eloquent exposition of this topic and the associated difficulties in both theory and experiment. The difficulty arises from the *orientational degeneracy of nematic liquids at rest*: whereas the degree of nematic orientation is uniquely specified by polymer concentration, the distinguished uniaxial director (primary axis of orientation) lies arbitrarily on the unit sphere (two continuous degrees of freedom), and the remaining two directors lie arbitrarily in the plane orthogonal to the primary director (one more degree of freedom). Equivalently, there are *three* zero eigenvalues of the linearized equations about nematic equilibria, corresponding to a three-dimensional center manifold which must be tracked as the degeneracy is broken by an applied perturbation, here a shear flow. Seminal kinetic theory results in weak flow are attained by Semenov, Kuzuu and Doi [110, 69, 70, 111]. We now explain our results on the shear-selection process for the mesoscopic tensor theory, and defer further details to a mathematical paper. Because the center manifold is so large, many scenarios are possible depending on the type of perturbation.

Recall that nematic equilibria at rest exist for $N > \frac{8}{3}$; they are uniaxial with director, say \mathbf{n}_1 , that lies arbitrarily on the unit sphere. From (9), uniaxiality implies $d_2 = d_3$, or $\beta = 0$. The degrees of orientation are uniquely specified by either d_1 or $s = \frac{1}{2}(3d_1 - 1)$, which are determined by the critical points of (33). (The isotropic state $s = 0$ exists for all concentrations N , and is unstable for $N > 3$.) The lower nematic state $s = s_- = \frac{1}{4}[1 - 3\sqrt{1 - \frac{8}{3N}}]$ exists for $N > \frac{8}{3}$, but is always an unstable saddle in the order parameter space (s, β) [43]. The upper nematic state $s_+ = \frac{1}{4}[1 + 3\sqrt{1 - \frac{8}{3N}}]$ is *always stable* in the order parameter subspace (s, β) . (The I-N transition surrounds $N = \frac{8}{3}, 3$.)

For this paper we fix a high concentration, $N = 6$, where $s_- \approx -.309$ and $s_+ \approx .809$, which takes further complexity associated with the I-N phase transition completely out of

the picture. We are now in position to explain for the modified Doi closure with $N = 6$, $|a| = 1$, **precisely seven steady states are selected as the flow is turned on**, $Pe \approx 0$: three states emerge from each of s_+ , s_- , and a single state emerges from the isotropic state. These results are schematically indicated in Figure 6, which we now explain. The first issue is state selection, then stability rests upon the fate of the three zero linearized eigenvalues.

Consider s_+ first. By continuous dependence of linearized eigenvalues in the weak flow limit, $Pe \approx 0$, we know that *equilibria shear-selected from s_+ are the only candidates for stable solutions!* (Caution: for finite shear rates, initially unstable branches can and do emerge as stable states; this is why even unstable branches require identification.)

The uniaxial director associated with s_+ lies anywhere on the sphere for $Pe = 0$. For the modified Doi model, Figure 2a shows (denoted by asterisks) the nematic equilibria at rest associated with $s_+ = .809$ on three independent uniaxial axes: $(0, s_+)$, $(s_+, 0)$, $(-s_+, -s_+)$. Note all three lie within the steady region \mathbf{S} for $|a| = 1$, while for $|a| = .8$ two reside in the unsteady region \mathbf{U} . Thus for $|a| = 1$ the weak shear limit selects three discrete, steady, major directors, denoted $\mathbf{n}^{(1)}$, $\mathbf{n}^{(2)}$, $\mathbf{n}^{(3)}$ (Figure 6): two are in-plane, given by (35); further stability analysis reveals **one stable flow-aligned state** and **one unstable flow-aligned state**. The third director aligns with the vorticity (z) axis called a **logrolling state**, which is **unstable** with a director instability of growthrate proportional to Pe . A different director representation is needed to capture the logrolling selection criterion; it is straightforward and omitted.

Next, the equilibria associated with s_- , depicted in Figure 2a along the three uniaxial axes, all reside in the steady region. For $Pe \approx 0$ the same arguments above give: **three unstable steady states emerge from s_-** . **Lastly,** the isotropic state clearly lies within the steady region, it is non-degenerate, so **a unique unstable state emerges from the isotropic phase**.

The vertical axis of Figure 6, $\|\mathbf{Q}\|$, is a special choice of “norm of \mathbf{Q} ” chosen to *highlight in-plane from out-of-plane states*: in-plane states with identical order parameters have the same norm, but out-of-plane directors yield a lower norm. We caution this is not the usual $\|\mathbf{Q}\|_2^2 = \mathbf{Q} : \mathbf{Q}$ definition, which is invariant under arbitrary director rotations and so would not provide the desired distinction. Our modified norm is used in all flow-phase diagrams in order to distinguish in-plane and out-of-plane mode selection. In Figure 6, the two in-plane directors associated with s_+ in the limit of $Pe = 0$ yield the same norm; the vorticity-aligned director yields a smaller norm. The same holds true for the three directors associated with s_- . When we plot solution branches vs. shear rate (Pe) in the figures to follow, for each of $s_{+,-}$, two branches of in-plane solutions emerge at the same $\|\mathbf{Q}\|$ height, another out-of-plane branch at slightly lower norm.

Summarizing: for $Pe \approx 0$, $N = 6$, and sufficiently large aspect ratios $|a| \approx 1$, this analysis explains how *seven solution branches* emerge for this closure scheme, yet with a unique stable, in-plane, flow-aligned monodomain. (The Rey-Tsuji closure will duplicate seven branches, the other Doi-HL closures will have slight differences as described below.) Solution branches in Figure 6 and all future figures are **color coded**: *green and black indicate stable states, blue and red indicate unstable states*; the unique stable state in the weak shear limit is flow-aligning.

Variations in state selection and stability due to closure scheme in the weak shear limit:

- The Doi and Rey-Tsuji closures, for sufficiently extreme molecule aspect ratios $r < \frac{1}{4}$ or $r > 4$ and fixed concentration $N = 6$, select only steady states: one stable in-plane flow-aligned state, three unstable in-plane states, two unstable logrolling states, and a nearly isotropic unstable state. Unsteady transitions begin at slightly less extreme aspect ratios, as Figures 2a,b convey.
- For the Rey-Tsuji closure and nematic concentrations $N > 6.5$, no steady states associated with s_+ survive, in-plane nor logrolling, for infinite or finite aspect ratio. By contrast, the Doi (Figure 2a) and HL1,2 (Figure 2c,d) closures *always preserve* the vorticity-aligned s_+ state in the weak shear limit. The logrolling state is never stable in the Doi or Rey-Tsuji model, but *always stable in both HL closures*.
- For both HL closures, the two potential in-plane solutions associated with s_+ for $Pe \approx 0$ are *always unsteady* for any aspect ratio, infinite or finite; the number and type of time-dependent states differ for the HL1 and HL2 closures:
 - The HL1 closure generates in-plane tumbling motions for both in-plane s_+ states, and the two orbits reproduce one another! This explains why the total multiplicity of solution branches for $Pe \approx 0$ drops from seven to six. The tumbling solution is unstable until large Pe , and the logrolling state is the unique attractor for small Pe .
 - The HL2 closure produces one tumbling in-plane solution (stable for low Pe), but another s_+ state tilts out-of-plane to create an *unstable kayaking* solution of type \mathbf{K}_2 , which by the symmetry (28) is a pair of unstable kayaking modes. The total multiplicity therefore jumps to eight, with four states emerging from s_+ , three from s_- . We deduce *bistability* for small Pe of a logrolling steady state and a tumbling in-plane monodomain.

All solution branches associated with s_- for $|a| > .8$ are always inside the steady region for all four closures, thus always emerge for $Pe \approx 0$ as unstable equilibrium branches, two

in-plane and one logrolling. The isotropic state always yields a unique unstable branch, for any closure and value of a .

In summary, the orientational degeneracy for large aspect ratio nematic liquids is broken in the limit of weak shear to yield seven or six solution branches, corresponding to between six and eight distinct monodomain solutions with either a unique or bi-stable attractor, whose *continuation* for finite shear rates and finite aspect ratios is developed next.

5 Flow-phase diagrams and transition phenomena for the eight mesoscopic models

We now present results for the eight closure models, which complement prior results of [112] for finite aspect ratio ($r = \frac{1}{3}$) discotics at high nematic concentration ($N = 6$). Flow-phase diagrams typically address stable solutions; many stable solutions emerge at critical shear rates or aspect ratios from unstable states, so we will give *all* stable and unstable solutions in the bifurcation diagrams, followed by Tables that list only the attractors vs. shear rate. Solutions are characterized according to two criteria: in-plane or out-of-plane, and mode type. The *in-plane* states are denoted: **FA** for flow-aligning, **W** for wagging, **T** for tumbling; out-of-plane states include the steady logrolling **LR** state, two types of kayaking **K** modes defined next, and chaotic orbits.

Larson and Ottinger introduced the term "kayaking" for out-of-plane solutions in which the major director rotates around the vorticity axis, akin to an Eskimo kayaker's paddle. We distinguish *two basic kayaking modes* which have distinct physical features. **K₁** is the Larson-Ottinger Eskimo paddle motion (Figure 3a); it is a periodic extension of the logrolling state. **K₂** characterizes major director rotations about an axis strictly *between* the vorticity axis and the shear plane (Figures 3b,4a). From Column 2 of Figures 3 and 4, we draw analogy from Lissajous figures. For the **K₁** mode, the major director rotates once per period around the vorticity axis; the reflection symmetry (28) of the entire **K₁** orbit reproduces itself. The **K₂** modes, by (28), occur in pairs. There is a "fundamental" in which every director rotates once per period (Figure 4a); there are "higher harmonic" **K₂** mode pairs in which each director executes an even number of loops per period (Figure 3b), shown below to result from period-doubling bifurcations of **K₂** attractors. To our knowledge, period-doubled modes were first discovered by Singh and Rey [112]; their pair symmetry and source of frequent bi-stability, and their role in a period-doubling bifurcation sequence to chaos are, to our knowledge, new.

We emphasize that *this nomenclature is based on director motion*, whereas the amplitude of order parameter motion varies considerably across the different monodomain attractors; it

is this latter feature that impacts whether the aforementioned scaling property of L-E theory is approximately satisfied. In Figures 3-5: Column 1 is a time lapse of the full orientation ellipsoid, with the projection onto the shearing plane for out-of-plane modes; Column 2 is the time lapse trace on the unit sphere of the major director in blue, and the minor directors in green and red for out-of-plane modes; Column 3 is the motion of the order parameter pair (s, β) . All solutions in this study are calculated using the software XPPAUT [37] written by G. B. Ermentrout, in which AUTO95 [28] was incorporated, and then confirmed and visualized with AUTO97 [29] and the commercial software packages Matlab and Maple.

5.1 Stable monodomains for extreme aspect ratios, $|a| \approx 1$ [121]

At high concentrations ($N = 6$), in weak shear ($Pe \approx 0$), for extremely large aspect ratios ($|a| \approx 1$), Figures 2,6 and surrounding arguments explain the multiplicity and stability of all monodomain solutions for each of the closure models. Bifurcation software confirms our analysis and tracks all solution branches and their stability for all Pe . We first summarize the robust stable monodomain features for large aspect ratios [121]:

- The Doi closure, for either rotational diffusivity form (21), and all normalized shear rates $Pe > 0$, yields a unique, in-plane, flow-aligned attractor **FA**. This prediction is consistent with L-E theory in the flow-aligning Leslie viscosity regime.
- The Rey-Tsuji closure with $|a| = 1$ yields qualitatively similar results to the Doi closure, a unique **FA** attractor.
- The HL1 closure has a richer flow-phase diagram for $|a| = 1$ because of the weak-flow selection properties noted earlier: from s_+ , one stable **LR** state is selected but the other states are unsteady and unstable. The results with either rotary diffusivity (21) are robust, so we give approximate Pe transition values for the orientation dependent case: a unique stable **LR** state for $0 < Pe < \approx 20$; bistable states (**T,LR**) for $20 < Pe < 45$; bi-stable (**T, K₁**) for $20 < Pe < 70$; then a unique in-plane **T**, giving way to a **W** attractor. Three bifurcations occur:
 - at $Pe \approx 20$, an unstable-to-stable **T** transition through a period-halving bifurcation (the tumbling period halves), remaining stable out to very high Pe ; note that the **T-W** transition is not a bifurcation;
 - at $Pe \approx 45$, the **LR** mode destabilizes through a Hopf bifurcation into a stable **K₁** branch;
 - at $Pe \approx 70$, the **K₁** branch destabilizes, leaving a unique attractor.

- The HL2 closure is robust for either rotary diffusivity form, selecting a stable **LR** steady state for all Pe . In contrast with HL1, the unsteady **T** mode is stable for HL2 at low and high Pe , losing stability for a range of Pe through period-doubling bifurcations at $Pe \approx 7$ and $Pe \approx 15$. There is a very narrow window of stable kayaking solutions with orientation-dependent rotary diffusivity near the first period-doubling bifurcation. The result is bi-stable, tri-stable, or unique stable attractors for the HL2 model.

We move now to **finite aspect ratio predictions**.

5.2 The Modified Doi Model: constant rotary diffusivity & finite aspect ratios

Figure 7 shows the flow-continuation branches for each of the seven equilibria of Figure 6, for the *finite discotic aspect ratio* $r = \frac{1}{4}$ ($a = -\frac{15}{17}$), with $N = 6$ held fixed. (By the symmetry (26), this also yields the behavior of rodlike molecules of aspect ratio 4 : 1.) We find persistence of the Doi closure prediction for infinite aspect ratio rods and discs: the **FA** steady state is the unique stable attractor for all $Pe > 0$.

Next we *lower the aspect ratio to 3 : 1* ($|a| = \frac{8}{10}$), with results given in Figure 8 and Table 1, showing the *flow response and transition phenomena are dramatically different in the weak shear regime*. We describe this, and only this, flow diagram in detail, for two reasons: first, it is the most complex and captures a diversity of stable monodomain motions; and second, many generic bifurcations occur in this model which offer concrete examples of possible physical transition behavior. The attractors vs. shear rate are listed in Table 1; representative monodomain attractors are imaged in Figures 3,4,5.

First we clarify the solution branches in Figure 8 and subsequent bifurcation diagrams. The vertical axis consists of some "amplitude", which for unsteady solutions requires a choice. In Figure 8a, we use the time-average of $\|Q\|$ defined in Figure 6, over one period for periodic solutions or over a sufficiently long time for aperiodic motion. In Figure 8b, we give the maximum and minimum values for one out-of-plane component, Q_{yz} , associated with each branch in Figure 8a; in-plane solution branches all have $Q_{yz} = 0$, whereas non-zero values flag out-of-plane states. We give both min and max values of Q_{yz} to illustrate out-of-plane orbits never cross the shearing plane.

- At low shear rates, $0 < Pe < 3.72$, *no stable steady states exist*, as explained earlier surrounding Figure 2a for this lower aspect ratio. The weak shear limit with aspect ratio $r = 3$ is therefore qualitatively different than with aspect ratios larger than $r = 4$.

- For sufficiently high shear rates, $Pe > 3.72$, the stable **FA** branch is recovered as the *globally attracting monodomain*, indicating only quantitative changes due to aspect ratio for sufficiently strong shear in this model.

We now highlight the distinctive weak-shear features from Figure 8 and Table 1:

- For $0 < Pe < 2.162$, the unique attractor is a classical kayaking mode **K₁**, shown as the green dotted branch in Figures 8a,b; one of these stable monodomains is visualized in Figure 3a for $Pe = 2$. The ellipsoid shape distortions (governed by the order parameter projection in Column 3) are small amplitude, suggesting reasonable approximation by a L-E director theory.
- In Figure 8, the top three solution branches (red dashed **T**, green dotted **K₁**, blue solid **LR**) are the states selected for $r = 3, \frac{1}{3}$ when the orientational degeneracy of the nematic equilibrium s_+ is broken for $Pe \approx 0$.
- A comparison of aspect ratios $r = 3, 4$ (or $\frac{1}{3}, \frac{1}{4}$) is deduced from Figures 2a, 7, 8: the **LR** state is common for both aspect ratios, and unstable; the two in-plane flow-aligned states emerging from s_+ for $r = 4$ have transitioned into unsteady solutions, a stable **K₁** mode and an unstable, in-plane **T** mode.
- These steady-to-unsteady transitions due to aspect ratio changes between $r = 4$ and $r = 3$ are only understood by treating the aspect ratio as a bifurcation parameter. To do so for the entire flow-phase diagrams linking Figures 7 and 8 is numerically prohibitive and would consist of 7 sheeted surfaces that fold and intersect several times! We therefore settle for a slice of this picture at fixed Pe , illustrated in Figure 9 for $Pe = 3.2$ and a range of discotic aspect ratios. The main feature of Figure 9 to notice is that the **FA** stable branch is the *only solution branch at $Pe = 3.2$* , but by freezing Pe and N and varying the aspect ratio only, a complex sequence of bifurcations unfolds before the phase diagram settles into the stable **K₁** branch observed in Figure 8 at $a = -0.8$ or $r = 3$.
- The structure of the four lower, unstable branches of Figures 7 and 8 is robust, corresponding to unstable, steady solutions arising in the weak shear limit from s_- and the isotropic state.

These remarks address the weak shear limit and the states that break nematic orientational degeneracy. Next we address the finite Pe -dependent continuation of these solution branches.

- The branch of **stable \mathbf{K}_1** solutions persists until $Pe \approx 2.923$, clearly visible from the Q_{yz} projection in Figure 8b. $Pe \approx 2.923$ is a saddle-node bifurcation, with the kayaking branch reversing back for lower Pe as an unstable \mathbf{K}_1 branch. This unstable periodic branch, as Pe is lowered, approaches in-plane motion, undergoing a period-halving bifurcation at $Pe \approx 2.162$, just as it connects to the previously unstable, in-plane **T** branch. This structure yields the *second stable T/W state listed in Table 1* for $2.162 < Pe < 2.405$, which is tumbling at the low end and wagging at the high end of these shear rates. Thus this interval has **bi-stable attractors**. Their respective domains of attraction are not addressed here.
- A stable **W** mode is depicted in Figure 5, which we also use to illustrate the rod-discotic correspondence (26). Note the significant order parameter oscillations (Column 3), reflected in the shape distortions of the orientation ellipsoids (Column 1). Such behavior is suppressed in a L-E description.
- At $Pe \approx 2.405$, the stable **W** mode bifurcates out-of-plane, creating a **pair of stable, periodic \mathbf{K}_2** modes, one on either side of the shearing plane by virtue of the reflection symmetry (28). One orbit is visualized in Figure 4a for $Pe = 2.5$. Note the significant order parameter oscillations, not captured by a L-E approximation. The energy of this attractor is equally shared between director and order parameter oscillations. From Table 1 we find **tri-stability** for a short band of shear rates, $2.405 < Pe < 2.536$.
- At $Pe \approx 2.536$, a cascade of period doubling bifurcations of the double- \mathbf{K}_2 branch takes place over a very short range of Pe . The period-doubling sequence leads rapidly into a chaotic attractor.
- One also enters this chaotic range of Pe from higher shear rates by following the bifurcations of the unique **FA** branch as Pe drops below 4. At $Pe \approx 3.717$, a Hopf bifurcation of the steady **FA** branch leads to a stable, out-of-plane, periodic double- \mathbf{K}_2 branch. Figure 8a shows this as a single branch, while Figure 8b shows both the max and min of Q_{yz} over a period. The symmetric mode tilted oppositely from the shearing plane has values $-Q_{yz}$, not shown here.
- The \mathbf{K}_2 branch persists for $Pe < 3.717$ until approximately 3.29 when the first period doubling bifurcation occurs, giving way to a new branch of stable \mathbf{K}_2 solutions. As shown in Figure 3b for $Pe = 3.27$, each director executes a double loop in each period; the successive period-doublings yield four loops, then eight, etc.

- The period-doubled \mathbf{K}_2 monodomains tightly oscillate about the average director alignment, with visible shift of energy into the order parameters marked by shape distortions of the orientation ellipsoids. This behavior is not possible within L-E models.
- This bifurcation marks the onset of a period-doubling cascade to a chaotic attractor by $Pe \approx 3.245$. Figure 10 is a blow-up of four such period doubling bifurcations. Just below $Pe = 3.245$ all out-of-plane data converge to the chaotic attracting state. In-plane data cannot escape the shearing plane without an infinitesimal perturbation out-of-plane.
- Figure 4b visualizes the chaotic attractor for $Pe = 3.2$ with significant director and order parameter variations. The motion consists of random jumping between the two fundamental kayaking modes, \mathbf{K}_1 and \mathbf{K}_2 . An explanation of this chaotic attractor in terms of a symbol sequence of these two modes seems plausible; an analytical description of this chaotic attractor presents a nice dynamical systems problem.
- Table 1 summarizes the Modified Doi Model predictions of stable monodomains versus Pe : a unique attractor at low and sufficiently large shear rates, bi-stable and tri-stable periodic motions in a range of low shear rates, and a narrow window of weak shear rates with chaotic response.

The regime we call “chaotic” has to be substantiated by detailed statistics. We have confirmed irregular Poincare maps and positive Lyapunov exponents; e.g., an exponent of .005 is calculated for the Figure 4b attractor. These diagnostics and bifurcation scenario are consistent with Grosso et al. [52], who computed the bifurcation diagram of the Smoluchowski pde of the Doi kinetic theory with infinite aspect ratio using AUTO97. This similarity between our finite aspect ratio quadratic closure model and their infinite aspect ratio full kinetic theory compels further investigation.

Table 1: Stable and chaotic solutions of the Modified Doi model

Range of Pe	(0, 2.162)	(2.162, 2.405)	(2.405, 2.536)	(2.536, 2.923)
Solution type	\mathbf{K}_1	$\mathbf{K}_1, \mathbf{T}/\mathbf{W}$	$\mathbf{K}_2^{+,-}, \mathbf{K}_1$	$\mathbf{K}_1, \text{Chaos}$
Range of Pe	(2.923, 3.245)	(3.245, 3.717)	(3.717, 6)	
Solution type	Chaos	$\mathbf{K}_2^{+,-}$	FA	

5.3 Modified Doi Model with orientation-dependent rotary diffusivity

With orientation-dependent diffusivity, the flow-phase diagram (Figure 11) of the modified Doi model simplifies considerably, altering some fundamental predictions regarding sta-

ble attractors (Table 2). Recall that our generalized Leslie criterion for steady vs. unsteady selection in the weak flow limit was independent of rotary diffusivity (21); note the number, mode type, and stability of monodomains for $Pe \approx 0$ are identical for both Modified Doi Models. In particular, the features robust to the choice (21) are:

- The \mathbf{K}_1 monodomain is the unique attractor for low shear, disappearing through a saddle-node bifurcation at moderate shear rate.
- The unstable \mathbf{T} branch at low Pe period-halves to create a stable \mathbf{T}/\mathbf{W} branch, overlapping for some range of Pe with the \mathbf{K}_1 attractor (a bi-stable region).

However, several important changes due to orientation-dependent rotary diffusivity are predicted:

- The stable \mathbf{T}/\mathbf{W} branch persists for very high Pe , leading to a unique, unsteady, in-plane wagging monodomain at sufficiently high shear rates, versus a unique, steady flow-aligned state with constant diffusivity.
- Since the emergence of \mathbf{K}_2 bi-stable pairs and the period-doubling cascade to chaos for constant diffusivity arise from bifurcations of the \mathbf{T}/\mathbf{W} branch, that entire transition scenario is destroyed with \mathbf{Q} -dependent diffusivity. Neither the \mathbf{K}_2 nor chaotic attractors are predicted.

Table 2: Stable solutions of the Modified Doi Model with orientation-dependent rotary diffusivity

Range of Pe	$(0, 7.115)$	$(7.115, 9.923)$	$(9.923, 20)$
Solution type	\mathbf{K}_1	$\mathbf{K}_1, \mathbf{T}/\mathbf{W}$	\mathbf{T}/\mathbf{W}

5.4 Doi-Rey-Tsuji Model

Figure 12 depicts the bifurcation diagram of the Doi-Rey-Tsuji Model with constant rotary diffusivity; Table 3 describes the stable monodomains versus Pe . Surrounding Figure 2 we explained how the weak flow limit, $Pe \approx 0$, yields the same selection criteria of steady and unsteady states from the nematic equilibria $s_+, s_-, 0$ for the Doi and Rey-Tsuji closures. Comparison of Figures 8, 12 shows even stronger agreement, indeed almost identical transition phenomena apart from the small chaotic band:

- All seven solution branches that emerge for $Pe \approx 0$ match, in type and stability!
- The unique stable attractor in the start-up of shear is a \mathbf{K}_1 orbit.

- The low shear, unstable **T** branch undergoes a period-halving bifurcation into a stable **T/W** branch, yielding bi-stability with the **K₁** monodomain.
- The stable **T/W** branch bifurcates out-of-plane, creating a pair of stable **K₂** modes, and a shear-rate interval of tri-stability.
- The stable **K₁** branch loses stability in a saddle-node bifurcation at intermediate shear rates, never to emerge again.
- The high shear-rate attractor is the steady, in-plane **FA** state.

The noteworthy qualitative difference between the Modified Doi and Doi-Rey-Tsuji Models centers upon how the **K₂** symmetric pairs bifurcate and lose stability, which is an extremely subtle phenomenon, yet predicted in both models to occur over approximately one dimensionless shear-rate unit.

Table 3: Stable solutions of the Doi-Rey-Tsuji Model

Range of Pe	(0, 1.813)	(1.813, 2.207)	(2.207, 3.356)
Solution type	K₁	K₁, T/W	K₁, K₂^{+, -}
Range of Pe	(3.356, 3.375)	(3.375, 8.856)	(8.856, 10)
Solution type	K₁	K₁, FA	FA

5.5 Doi-Rey-Tsuji Model with orientational diffusivity

The flow-phase diagram (Figure 13) and stable attractors (Table 4) are qualitatively similar to the Modified Doi Model (Figure 11, Table 2) with orientational diffusivity. The only meaningful differences are quantitative, and the transition scenarios are remarkably consistent: a unique **K₁** attractor in start-up, bi-stable with a **T/W** mode for some intermediate shear rates, then a unique stable **T/W** attractor in the high shear range.

Table 4: Stable monodomains of the Doi-Rey-Tsuji Model with non-constant rotary diffusivity

Range of Pe	(0, 4.955)	(4.955, 30.94)	(30.94, 40)
Solution type	K₁	K₁, T/W	T/W

The above four models were analyzed in two excellent papers by Singh and Rey [112], who worked at a fixed aspect ratio ($a = -0.8$) and fixed polymer concentration ($N = 6$) to study sheared discotic nematic liquids. Our simulations generalize theirs by allowing for variable aspect ratio, and by a more detailed resolution of the bifurcation diagrams captured by the software package XPPAUT of Ermentrout [37]. One consequence of our studies on the Doi

and Rey-Tsuji closures, with or without orientational rotary diffusivity, is that the logrolling steady state is always unstable. Yet, Larson and Ottinger found stable logrolling states in simulations of the Doi kinetic theory for infinite aspect ratio rods [73], which have been subsequently confirmed in detailed kinetic simulations by [38, 80, 83]. As shown by Figure 2 and the tensor selection criteria, the Hinch-Leal closures [58, 59, 60] preferentially select stable **LR** states in the weak shear limit, for all aspect ratios. We turn to their predictions for finite aspect ratio fluids.

5.6 Modified Doi-HL1 Model

Figure 14 and Table 5 depicts the bifurcation diagram and stable monodomains for shape parameter value $|a| = \frac{24}{26}$, corresponding to molecular aspect ratio $r = 5$ or $\frac{1}{5}$. The key features are:

- the **LR** state is the unique attractor at start-up of shear;
- the unstable **T** state stabilizes in a period-halving bifurcation, leading to bi-stable regimes for a range of Pe , first with **LR** then **K₁** monodomains;
- the **LR** state bifurcates to a **K₁** attractor in the most intuitively natural, steady-unsteady transition (Hopf bifurcation): the major director first aligns then oscillates about the vorticity axis as the shear rate increases;
- the **K₁** state is lost through a saddle-node bifurcation at an intermediate shear rate, and the unstable branch doubles back at lower shear to connect with the **T** branch precisely at the period-halving, stability transition;
- the observable attractors from Table 5 are, in terms of increasing shear rate, a unique **LR** state, then bi-stable **LR** and **T** states, then bi-stable **T** and **K₁** states, then a unique **T/W** branch of monodomains for high Pe ;
- the monodomain response is predicted to be steady at low shear, bi-stable steady and in-plane tumbling for a very narrow window of shear rates, then bi-stable transient states (one in-plane, another out-of-plane), and finally in-plane unsteady attractors at sufficiently high shear rates.

Table 5: Stable solutions of the Modified Doi-HL1 model with constant diffusivity

Range of Pe	(0, 7.509)	(7.509, 8.638)	(8.638, 15.85)	(15.85, 20)
Solution type	LR	LR, T/W	K₁, T/W	T/W

5.7 Modified Doi-HL1 Model with orientational rotary diffusivity

As detailed in Table 6, the incorporation of orientation-dependent rotary diffusivity for the HL1 closure scheme has no qualitative effect on the results for aspect ratios 5 and $\frac{1}{5}$. The quantitative effect is to shift all bifurcations to higher shear rates, so that the **LR** attractor is predicted to be the unique response until $Pe \approx 22$, and the bi-stable region lasts for a span of 48 in Pe . The basic bifurcation structure, however, is remarkably robust at this aspect ratio.

Table 6: Stable monodomains: Doi-HL1 Model with orientational diffusivity

Range of Pe	(0, 21.96)	(21.96, 47.82)	(47.82, 71.7)	(71.7, 80)
Solution type	LR	T/W, LR	T/W, K_1	T/W

5.8 Modified Doi-HL2 Models for either rotary diffusivity

The Modified Doi-HL2 Model is also robust to constant or orientation-dependent rotary diffusivity. The flow-phase diagram for constant diffusivity is given in Figure 15; Tables 7 and 8 indicate all stable monodomains vs. Pe . We choose aspect ratio 5 to compare the HL2 and HL1 closures.

The key features of the HL2 models are:

- The **LR** state is stable for all Pe !
- The in-plane **T** mode is stable at the start-up of shear, loses stability in an intermediate window of shear rates, then regains stability for all sufficiently high shear rates. The **T-to-W** transition, as always, occurs at some intermediate shear rate.
- At low and sufficiently high shear rates, bi-stable **LR** and **T/W** states prevail; the internal window has only the **LR** attractor.
- The HL2 closure is seen to suppress stable kayaking monodomains, and indeed no unsteady out-of-plane motion is stable.

Table 7: Stable solutions of the Modified Doi-HL2 model with constant diffusivity

Range of Pe	(0, 2.034)	(2.034, 8.179)	(8.179, 20)
Solution type	LR, T/W	LR	LR, T/W

Table 8: Stable monodomains: Doi-HL2 Model with orientational diffusivity

Range of Pe	(0, 6.528)	(6.528, 16.48)	(16.48, 40)
Solution type	LR, T/W	LR	LR, T/W

6 Conclusion

The role of finite-aspect-ratio effects in monodomain response to simple shear, and to more general linear flows, has been studied from various tensor orientation models. Several symmetry properties were developed for mesoscopic Doi-type models, independent of closure approximation. These properties were used to develop intuition about finite-aspect-ratio nematic liquids in shear and related linear flows, and to extrapolate theoretical and experimental results from rods to discotics, and from finite aspect ratio fluids to extremely large aspect ratio fluids. Symmetries of a fixed aspect ratio fluid in simple shear were further used to explain necessary constraints on monodomain motion. E.g., a monodomain that tilts out-of-plane cannot return to in-plane orientation in finite time; all such motion has a mirror-reflection in the opposite direction out of the shearing plane, which leads to bi-stable kayaking modes whose major director oscillates between the vorticity axis and shearing plane. It will be interesting to explore whether such bi-stable attractors exist in laboratory experiments with model monodisperse nematic liquids; indeed, some closure schemes predict these attractors and others do not. All solutions and monodomain transitions versus shear rate and aspect ratio have been compared with Leslie-Ericksen model behavior; clearly, the tensor theories capture new properties and new phenomena which require experimental validation.

By exploring four different closure schemes, with and without orientational rotary diffusivity, we have shown that with finite-aspect-ratio effects, the Doi mesoscopic theory captures a diversity of monodomain features at fixed, high (nematic) concentrations:

- Weak-shear, monodomain selection mechanisms range from steady to unsteady, in-plane to out-of-plane, unique to bi-stable or even tri-stable; these features are sensitive to closure scheme and molecular aspect ratio.
- Shear-dependent transition scenarios likewise are strongly sensitive to closure scheme and molecular aspect ratio.

Many, but each intuitively plausible, scenarios are detailed. This diversity of mesoscopic behavior is consistent with an interpretation that a "monodisperse finite-aspect-ratio fluid" and second-moment closure scheme play the role of broad-brush fitting parameters for laboratory nematic fluids. Macromolecular fluids are always polydisperse with statistical aspect-ratio distributions. The Maier-Saupe potential employed here assumes a single parameter (dimensionless concentration N), short-range potential, which we have fixed in this study and suppressed its dependence on aspect ratio. The diversity of model behavior predicted in this paper reflects the diversity of experimental monodomain behavior of nematic polymers versus shear rate. We suppose that in restricted flow regimes, one can accurately accomplish

model fitting to monodomain states and nontrivial transition phenomena within this class of models. From a reasonable fit between experimental monodomain response and model predictions, one can then confidently proceed to model the onset of mesoscopic structure formation. The various observable transient monodomain states seen here, if confirmed in the laboratory, portend very different routes to subsequent mesostructure formation or flow instabilities, a topic which we are currently exploring with the current study as a guide.

Acknowledgment and Disclaimer

Effort sponsored by the Air Force Office of Scientific Research, Air Force Materials Command, USAF, under grant numbers F49620-99-1-0003 and F49620-00-1-0008. The US Government is authorized to reproduce and distribute reprints for governmental purposes notwithstanding any copyright notation thereon. The views and conclusions contained herein are those of the authors and should not be interpreted as necessarily representing the official policies or endorsements, either expressed or implied, of the Air Force Office of Scientific Research or the US Government.

References

- [1] Alderman, N.J., Mackley, M.R., *Mol. Cryst. Liq. Cryst.* **79**, 149 (1985).
- [2] Andrews, N.C., Edwards, B.J., McHugh, A.J., *J. Rheol.* **39**, 1161-1181 (1995).
- [3] Andrews, N.C. Edwards, B.J., McHugh, A.J., *J. Rheol.* **40**(3), 459-469 (1996).
- [4] Archer, L., Larson, R.G., *J. Chem. Phys.* **103**, 3108-3111 (1995).
- [5] Atkin, R.J., *Arch. Rational Mech. Anal.* **38**, 224 (1970).
- [6] Baek, S.G., Magda, J.J., Larson, R.G., *J. Rheol.* **37**, 1201 (1993).
- [7] Baek, S. G., Magda, J. J., Larson, R. G., *J. Rheol.* **38**, 1473 (1994).
- [8] Bachelor, G. K., *J. Fluid Mech.* **41**(3), 545-570 (1970).
- [9] Beris, A.N. and Edwards, B.J., **Thermodynamics of Flowing Systems with Internal Microstructure**, Oxford Science Publications (1994).
- [10] Berry, G.C., *Mol. Cryst. Liq. Cryst.* **165**, 333 (1988).
- [11] Berry, G.C., *J. Rheol.* **35**, 943 (1991).
- [12] Berry, G.C., Tan, Z., Rheological and rheo-optical studies of shear deformation on nematic solutions of poly(1,2-PET), preprint Univ. of Pittsburgh (2001).

- [13] Bhave, A.V., Menon, R.K., Armstrong, R.C., Brown, R.A., *J. Rheol.* **37**, 413-441 (1993).
- [14] Bird, B., Armstrong, R.C., and Hassager, O., **Dynamics of Polymeric Liquids**, Volumes 1, 2, John Wiley and Sons (1987).
- [15] Boudreau, D.M., Winter, H.H., Lillya, C.P., Stein, R.S., *Rheol. Acta* **38**, 503 (1999).
- [16] Bruinsma, R. Safinya, C.R., *Phys. Rev. A* **43**, 5377 (1991).
- [17] Burghardt, W.R., *Macromol. Chem. Phys.* **199**, 471 (1998).
- [18] Burghardt, W.R., Fuller, G.G., *J. Rheol.* **34**, 959-992 (1990).
- [19] Burghardt, W.R., Fuller, G.G., *Macromolecules* **24**, 2546 (1991).
- [20] Carlsson, T., *Mol. Cryst. Liq. Cryst.* **104**, 307-334 (1987).
- [21] Carlsson, T., Skarp, K., *Liquid Crystals* **1**, 455-471 (1986).
- [22] Chandrasekhar, S., **Liquid Crystals**, 2nd ed., Cambridge University Press (1992).
- [23] Chaubal, C.V., Leal, L.G., Fredrickson, G.H., *J. Rheol.* **39**, 73-103 (1995).
- [24] Chillingworth, D.R.J., Vicente Alonso, E., Wheeler, A.J., *J. Phys. A: Math. Gen.* **34**, 1393-1404 (2001).
- [25] Cladis, P.E., Torza, S., *Phys. Rev. Lett.* **35**, 1283 (1975).
- [26] Clar, M.G., Saunders, F.C., Shanks, I.A., Leslie, F.M., *Mol. Cryst. Liq. Cryst.* **70**, 195-222 (1981).
- [27] de Gennes, P-G, Prost, A., **The Physics of Liquid Crystals**, 2nd ed., Oxford University Press (1993).
- [28] Doedel, E. J. et al., **AUTO95: Continuation and bifurcation software for ordinary differential equations**, Concordia University (1995).
- [29] Doedel, E. J. et al., **AUTO97: Continuation and bifurcation software for ordinary differential equations**, Concordia University (1997).
- [30] Doi, M. *J. Polym. Sci., Polym. Phys. Ed.* **19**, 229 (1981).
- [31] Doi, M. and Edwards, S. F., **The Theory of Polymer Dynamics**, Oxford U. Press (Clarendon), London-New York (1986).
- [32] Donald, A.M., Windle, A.H., **Liquid Crystalline Polymers**, Cambridge Solid State Science Series, Cambridge University Press (1992).
- [33] Dupre', D.B., Techniques for the evaluation of material constants in lyotropic systems and the study of pretransitional phenomena in polymer liquid crystals, Chapter 7, **Polymer Liquid Crystals**, edited by Ciferri, A., Krigbaum, W., Meyer, R.B., Academic Press-New York (1982).
- [34] Edie, D., McHugh, J.J., *Carbon* **34**(11), 1315-1322 (1996).

- [35] Ericksen, J.L., Arch. Rat. Mech. Anal. **4**, 231 (1960).
- [36] Ericksen, J.L., Arch. Rat. Mech. Anal. **9**, 371 (1962).
- [37] Ermentrout, B., XPPAUT-the differential equation tool, University of Pittsburg, 2001.
- [38] Faraoni, V., Maffettone, P. L., J. Rheol. **43**, 829, (1999).
- [39] Farhoudi, Y., Rey, A.D., J. Rheol. **37**, 289-314 (1993).
- [40] Feng, J., Chaubal, C.V., and Leal, L.G., J. Rheol. **42**, 1095-1119 (1998).
- [41] Feng, J., Sgalari, G., Leal, L.G., J. Rheol. **44**, 1085-1101 (2000).
- [42] Feng, J., Tao, J., Leal, L.G., Roll cells and disclinations in sheared nematic polymers, Preprint (2001).
- [43] Forest, M.G., Wang, Q., Zhou, H., Physics Fluids **12**(3), 490-498 (2000).
- [44] Forest, M.G., Wang, Q., Zhou, H., Phys. Rev. E **61**(6), 6655-6662 (2000).
- [45] Forest, M.G., Wang, Q., Zhou, H., Liquid Crystals **28**(5), 717-720 (2001).
- [46] Forest, M.G., Wang, Q., Zhou, H., Physica D **152-153**, 288-309 (2001).
- [47] Fuller, G.G., **Optical Rheometry of Complex Fluids**, Oxford University Press, Oxford (1995).
- [48] Gahwiller, C., Phys. Rev. Lett. **28**, 1554-1556 (1972).
- [49] Golubitsky, M., University of Houston preprint (2001).
- [50] Gotsis, A.D., Baird, D.G., Rheol. Acta **25**, 275 (1986).
- [51] Grizzuti, N., Cavella, S, Cicarelli, P., J. Rheol. **34**, 1293 (1990).
- [52] Grosso, M., Keunings, R., Crescitelli, S., Maffettone, P.L., Prediction of chaotic dynamics in sheared liquid crystalline polymers, Preprint (2001) and lecture, Society of Rheology Annual Meeting, Hilton Head, SC, February (2001).
- [53] Han, C.D., Kim, S.S., J. Rheol. **38**, 13 (1994).
- [54] Han, W.H., Rey, A.D., Phys. Rev. E **50**, 1688-1691 (1994).
- [55] Han, W.H., Rey, A.D., J. Rheol. **38**, 1317-1334 (1994).
- [56] Hand, G. L., J. Fluid Mech. **13**, 33-46 (1962).
- [57] Hess, S. Z., Naturforsch. Teil **31A**, 1034 (1976).
- [58] Hinch, E.J., and Leal, L.G., J. Fluid Mech. **52**(4), 683-712 (1972).
- [59] Hinch, E.J., and Leal, L.G., J. Fluid Mech. **57**(4), 753-767 (1973).
- [60] Hinch, E.J., and Leal, L.G., J. Fluid Mech. **76**(1), 187-208 (1976).

- [61] Hongladarom, K., Burghardt, W., *Macromolecules* **26**, 785 (1993).
- [62] Hongladarom, K., Burghardt, W., Baek, S.G., Cementwala, S., Magda, J.J., *Macromolecules* **26**, 772 (1993).
- [63] Jeffery, G. B., *Proc. Roy. Soc. London Ser. A* **102**, 161-179 (1922).
- [64] Jenkins, J.T., *Ann. Rev. Fluid Mech.* **10**, 197-219 (1978).
- [65] Kiss, G., Porter, R.S., *J. Polymer Sci., Polym. Symp.* **65**, 193 (1978).
- [66] Kiss, G., Porter, R.S., *J. Polymer Sci., Polym. Phys. Ed.* **18**, 361 (1980).
- [67] Kroger, M., Sellers, H.S., *J. Chem. Phys.* **103**, 807-817 (1995).
- [68] Kupferman, R., Kawaguchi, M., Denn, M.M., *J. Non-Newt. Fluid Mech.* **91**, 255-271 (2000).
- [69] Kuzuu, N., Doi, M.J., *Phys. Soc. Japan* **52**, 3486-3494 (1983).
- [70] Kuzuu, N., Doi, M. J., *Phys. Soc. Japan* **53**, 1031 (1984).
- [71] Larson, R.G., Mead, D.W., *J. Rheol.* **33**, 1251 (1989).
- [72] Larson, R.G., *Macromolecules* **23**, 3983-3992 (1990).
- [73] Larson, R.G., Ottinger, H., *Macromolecules* **24**, 6270-6282 (1991).
- [74] Larson, R.G., Mead, D.W., *Liquid Crystals* **12**, 751 (1992).
- [75] Larson, R.G., Mead, D.W., *Liquid Crystals* **15**, 151 (1993).
- [76] Larson, R.G., **Rheology of Complex Fluids**, Oxford University Press (1998).
- [77] Leslie, F.M., *Arch. Rat. Mech. Anal.* **28**, 265 (1968).
- [78] Leslie, F.M., *Advances in Liquid Crystals* **4**, edited by H.G. Brown, Academic Press (1979).
- [79] Maffettone, P. L., *J. Non-Newt. Fluid Mech.* **45**, 339 (1992).
- [80] Maffettone, P.L., Crescitelli, S., *J. Rheol.* **38**, 1559 (1994).
- [81] Maffettone, P.L., Marrucci, G., *J. Non-Newt. Fluid Mech.* **38**, 273 (1991).
- [82] Maffettone, P.L., Marrucci, G., Mortier, M. Moldenaers, P. Mewis, *J. Chem. Phys.* **100**, 7736 (1994).
- [83] Maffettone, P.L., Crescitelli, S., *J. Non-Newt. Fluid Mech.* **59**, 73 (1995).
- [84] Magda, J.J., Baek, S-G, de Vries, L., Larson, R.G., *Macromolecules* **24**, 4460 (1991).
- [85] Manneville, P., *Mol. Cryst. Liq. Cryst.* **70**, 223-250 (1981).
- [86] Marrucci, G., Maffettone, P.L., *Macromolecules* **22**, 4076-4082 (1989).

- [87] Marrucci, G., Maffettone, P.L., *J. Rheol.* **34**, 1217-1230, 1231-1244 (1990).
- [88] Marrucci, G., *Macromolecules* **24**, 4176-4182 (1991).
- [89] Marrucci, G., Greco, F., *Mol. Cryst. Liq. Cryst.* **206**, 17-30 (1991).
- [90] Marrucci, G., Greco, F., *J. Non-Newt. Fluid Mech.* **44**, 1-14 (1992).
- [91] Marrucci, G., Greco, F., *Adv. Chem. Phys.* **86**, 331-404 (1993).
- [92] Mather, P.T., Pearson, D.S., Burghardt, W.R., *J. Rheol.* **39**, 627-648 (1995).
- [93] Mather, P.T., Pearson, D.S., Larson, R.G., *Liquid Crystals* **20**(5), 527-538 (1996).
- [94] Mather, P.T., Pearson, D.S., Larson, R.G., *Liquid Crystals* **20**(5), 539-546 (1996).
- [95] Mather, P.T., Romo-Uribe, A., Han, C.D., Kim, S.S., *Macromolecules* **30**, 7977 (1997).
- [96] Meiboom, S., Hewitt, R.C., *Phys. Rev. E* **30**, 261-263 (1973).
- [97] Moldenaers, P., Mewis, J., *J. Rheol.* **30**, 567 (1986).
- [98] Moldenaers, P., Ph.D. Thesis, Katholieke Universiteit Leuven (1987).
- [99] Moldenaers, P., Fuller, G., Mewis, J., *Macromolecules* **22**, 960 (1989).
- [100] Muller, J.A., Stein, R.S., Winter, H.H., *Rheol. Acta* **33**, 473 (1994).
- [101] Muller, J.A., Stein, R.S., Winter, H.H., *Rheol. Acta* **35**, 160-167 (1996).
- [102] Navard, P., *J. Polym. Sci., Polym. Phys. Ed.* **24**, 435 (1986).
- [103] Olmsted, P.D., Goldbart, P.M., *Phys. Rev. A* **41**, 4578 (1990).
- [104] Olmsted, P.D., Goldbart, P.M., *Phys. Rev. A* **46**, 4966 (1992).
- [105] Olmsted, P.D., Lu, C., *Phys. Rev. E* **56**, 55 (1997).
- [106] Pieranski, P., Guyon, E., *Phys. Rev. Lett.* **32**, 924-926 (1974).
- [107] Pradadarao, M., Pearce, E.M., Han, C.D., *J. Appl. Polym. Sci.*, **27**, 1343 (1982).
- [108] Rey, A.D., *Macromol. Theory Simul.* **4**(5), 857-872 (1995).
- [109] See, H., Doi, M., Larson, R.G., *J. Chem. Phys.* **92**(1), 792-800 (1990).
- [110] Semenov, A.N., *Sov. Phys. J.E.T.P.* **85**, 321-326 (1983).
- [111] Semenov, A.N., *Sov. Phys. J.E.T.P.* **66**, 712 (1986).
- [112] Singh, A.P., Rey, A.D., *Rheol. Acta* **37**, 30-45 (1998); **37**, 374-386 (1998).
- [113] Skarp, K., Carlsson, T., Lagerwall, T., Stebler, B., *Mol. Cryst. Liq. Cryst.* **66**, 199-208 (1981).

- [114] Srinivasarao, M., Berry, G.C., J. Rheol. **35**, 379 (1991).
- [115] Srinivasarao, M., Garay, R.O., Winter, H.H., Stein, R.S., Mol. Cryst. Liq. Cryst. **223**, 29 (1992).
- [116] Tseng, H.C., Silver, D.L., Finlayson, B.A., Physics Fluids **15**, 1213 (1972).
- [117] Tsuji, T. and Rey, A. D., J. Non-Newt. Fluid Mech. **73**, 127-152 (1997).
- [118] Van Horn, B.L., Winter, H.H., Rheol. Acta **39**, 294-300 (2000).
- [119] Volovik, G.E., JETP Lett. **31**, 273 (1980).
- [120] Wang, L., Rey, A.D., Liquid Crystals **23**(1), 93-111 (1997).
- [121] Wang, Q., J. Rheol. **41**(5), 943-970 (1997).
- [122] Wang, Q., J. Non-Newt. Fluid Mech. **72**, 141-162 (1997).
- [123] Wang, Q., A hydrodynamic theory for liquid crystalline polymers in proximity of spheroids, submitted to J. Chem Phys. (2000).
- [124] Wissbrun, K., J. Rheol. **37**, 777-797 (1993).
- [125] Yan, N.X., Labes, M.M., Baek, S.G., Magda, J.J., Macromolecules **27**, 2784-2788 (1994).
- [126] Yang, I.K., Shine, A.D., J. Rheol. **36**, 1079 (1992).
- [127] Zhou, W-J, Kornfield, J.A., Burghardt, W.R., Macromolecules **34**, 3654-3660 (2001).
- [128] Zhou, W-J, Kornfield, J.A., Ugaz, V., Burghardt, W.R., Link, D., Clark, N.A., Macromolecules **31**, 8474 (1999).
- [129] Zuniga, I., Leslie, F.M., Liquid Crystals **5**, 725-734 (1989).

Appendix: Viscosity coefficients

The results of Jeffery [63], Batchelor [8] as well as Hinch and Leal [58, 59] on ellipsoidal suspensions in a viscous solvent are utilized in the derivation of the viscous stress [123],

$$\begin{aligned}
 \eta_s &= \eta + 3/2\nu kT\zeta_3, \\
 \zeta_3 &= \frac{\zeta^{(0)}}{I_1}, \quad \zeta_1 = \zeta^{(0)}\left(\frac{1}{I_3} - \frac{1}{I_1}\right), \quad \zeta_2 = \zeta^{(0)}\left[\frac{J_1}{I_1 J_3} + \frac{1}{I_1} - \frac{2}{I_3}\right], \\
 I_1 &= 2r \int_0^\infty \frac{dx}{\sqrt{(r^2+x)(1+x)^3}}, \quad I_3 = r(r^2 + 1) \int_0^\infty \frac{dx}{\sqrt{(r^2+x)(1+x)^2(r^2+x)}}, \\
 J_1 &= r \int_0^\infty \frac{x dx}{\sqrt{(r^2+x)(1+x)^3}}, \quad J_3 = r \int_0^\infty \frac{x dx}{\sqrt{(r^2+x)(1+x)^2(r^2+x)}}.
 \end{aligned} \tag{37}$$

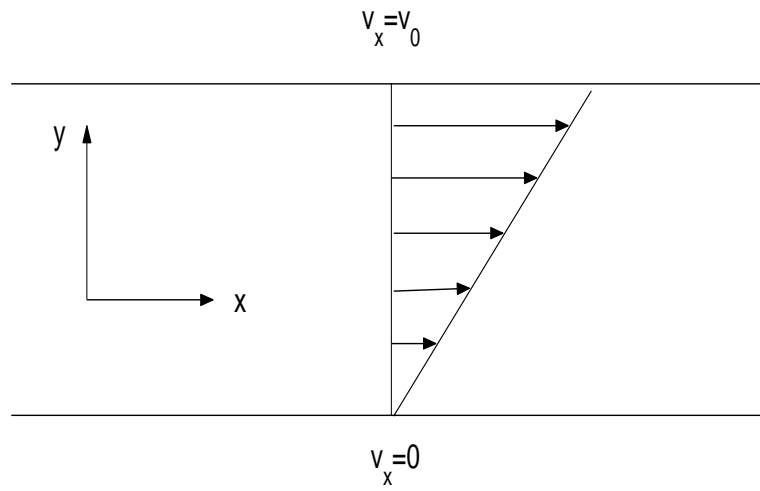


Figure 1: The shear flow geometry, where v_0 is the velocity of the moving plate: $v_0 = \dot{\gamma} \times (\text{width-between-the-plates})$.

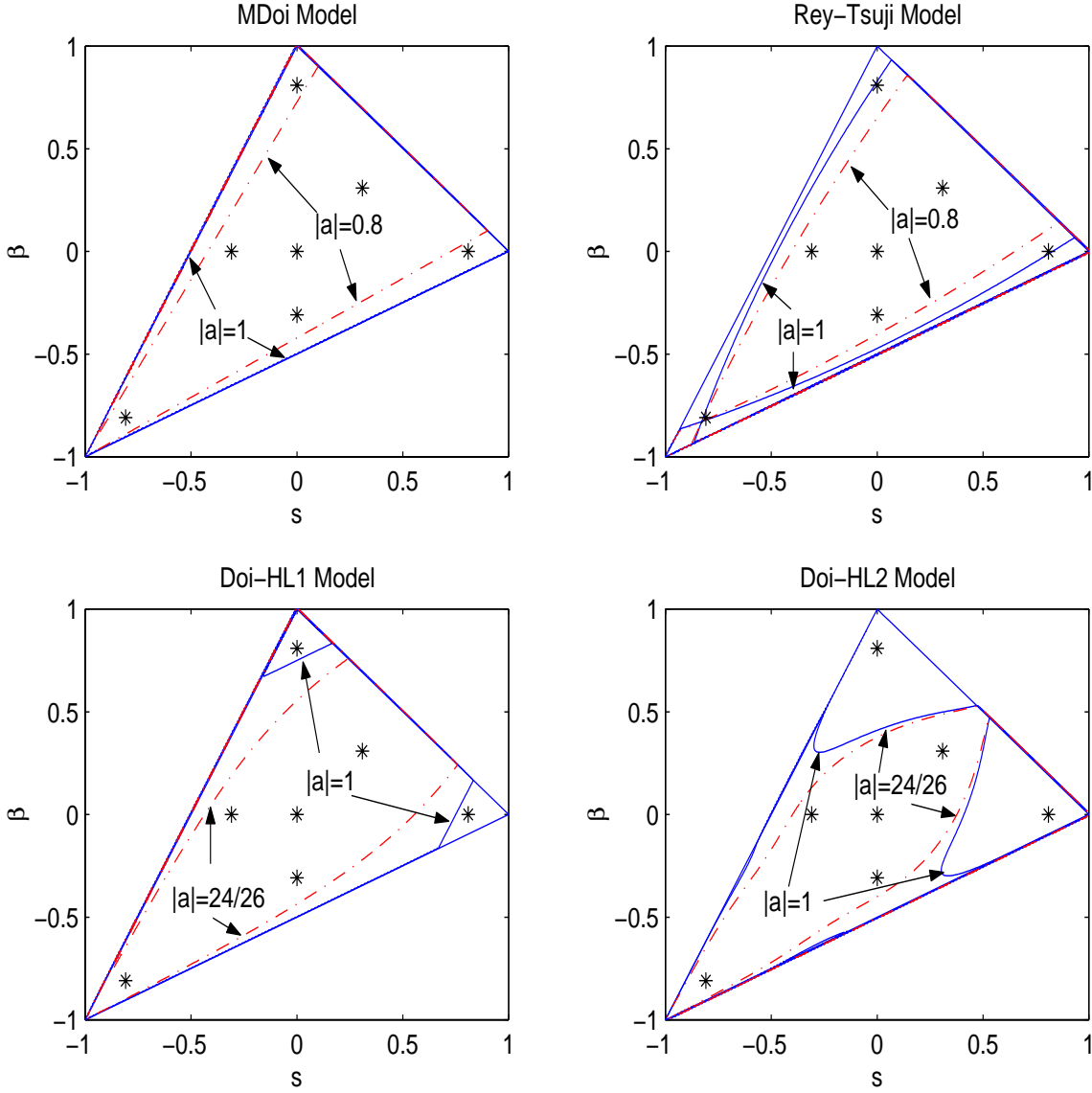


Figure 2: **Steady vs. unsteady selection criteria at the start-up of shear.** The triangle defined by solid lines and its interior are the admissible values of the order parameters (s, β) , a property of the orientation tensor \mathbf{Q} . For each of four closure rules, solid and dash-dotted curves are the transition boundaries separating steady and unsteady regions, and their dependence on aspect ratio. $|a| = 1$ corresponds to aspect ratio $r = 0$ or ∞ ; $|a| = 0.8$ corresponds to $r = 3, \frac{1}{3}$; $|a| = \frac{24}{26}$ corresponds to $r = 5, \frac{1}{5}$. Seven asterisks mark the quiescent equilibria specified by the fixed concentration $N = 6$. The horizontal and vertical axes correspond to in-plane director alignment, which persists in weak shear *if* the asterisk lies inside the steady region. The asterisks along the diagonal axis, $(-s_*, -s_*)$, correspond to a vorticity-aligned director, and determine whether steady logrolling states survive in weak shear.

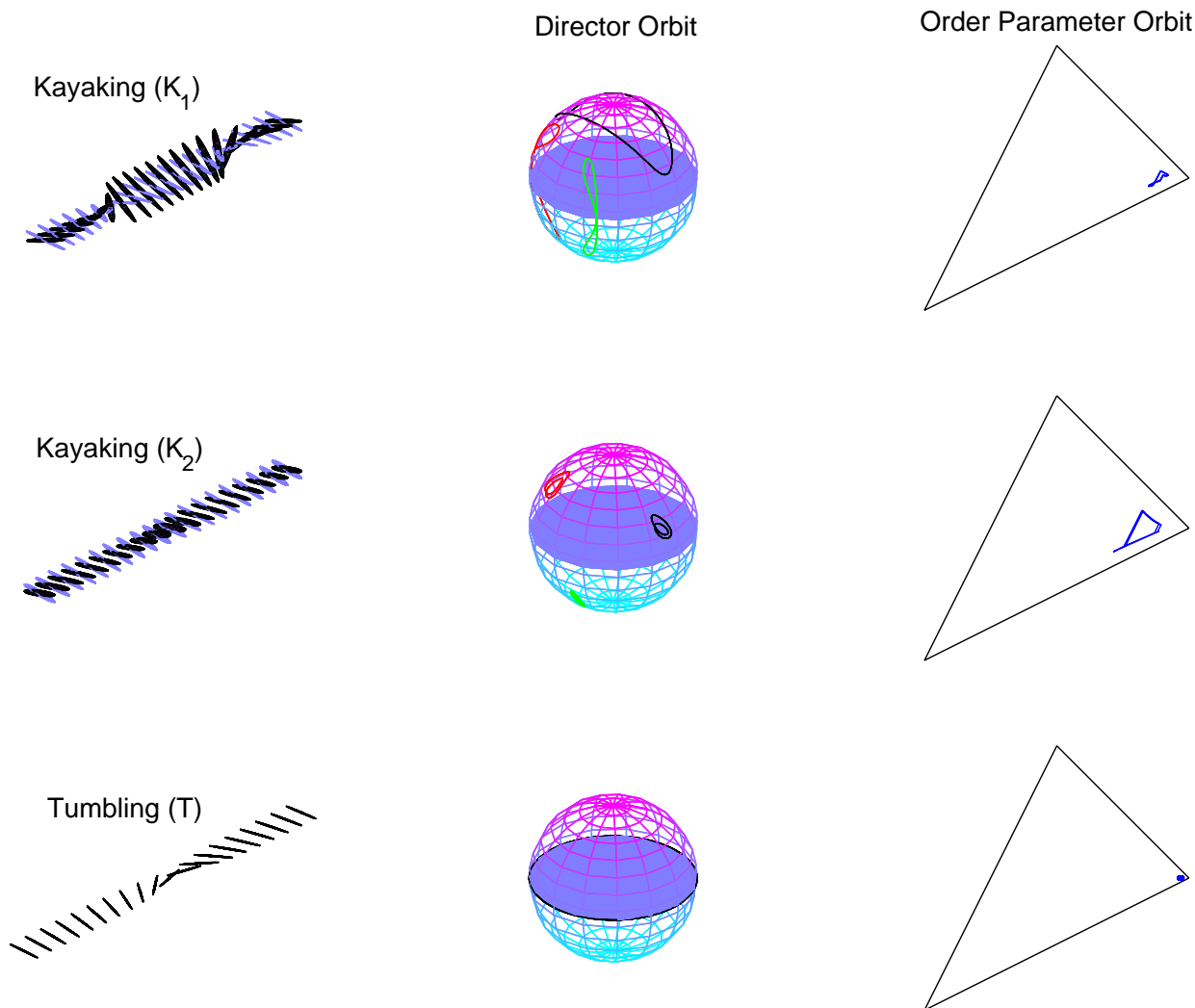


Figure 3: **Graphical representations of three prototypical monodomain attractors.** Top row: the Eskimo kayaking solution (\mathbf{K}_1) whose major director rotates around the vorticity axis. Middle row: a different kayaking solution (\mathbf{K}_2) whose major director rotates about an axis tilted between the vorticity axis and shearing plane; by symmetry arguments this motion is always accompanied by another kayaking solution tilted to the other side of the shearing plane. Last row: the in-plane tumbling solution (\mathbf{T} whose major director is in the shearing plane and tumbles with fixed period). Column 1 is a time lapse of the full orientation ellipsoid. Column 2 is a projection of each director on the unit sphere; the black trace is the major director, which is essentially the information contained in Leslie-Ericksen theory. Column 3 gives the order parameter (s, β) projection, characterizing shape changes of \mathbf{Q} . The two kayaking solutions are from the modified Doi model with discotic aspect ratio $r = \frac{1}{3}$ ($a = -0.8$), nematic concentration $N = 6$, and normalized shear rates $Pe = 2, 3.27$, respectively. The tumbling solution is from the modified Doi model with orientation-dependent rotary diffusivity, the same aspect ratio and concentration, but dimensionless shear rate $Pe = 14$.

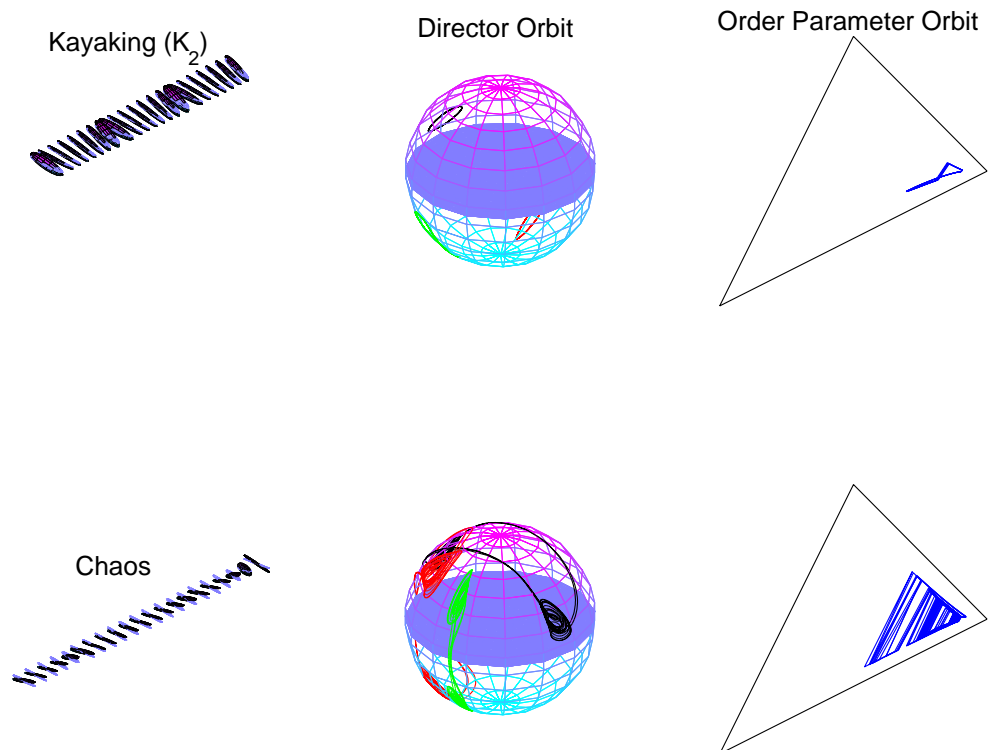


Figure 4: Graphical illustrations of additional stable monodomains: another \mathbf{K}_2 kayaking orbit, and a chaotic attractor. These solutions are from the modified Doi model with $N = 6$, $r = \frac{1}{3}$ and dimensionless shear rates: $Pe = 2.5, 3.2$ respectively. This kayaking orbit is distinguished from the other so-called \mathbf{K}_2 solution of the previous figure. Here there is a single fundamental period of oscillation, versus the double loop which arises from a period-halving bifurcation. More complex, multiple-looped motions on the sphere occur in the period-doubling cascade that occurs between the two attractors shown here.

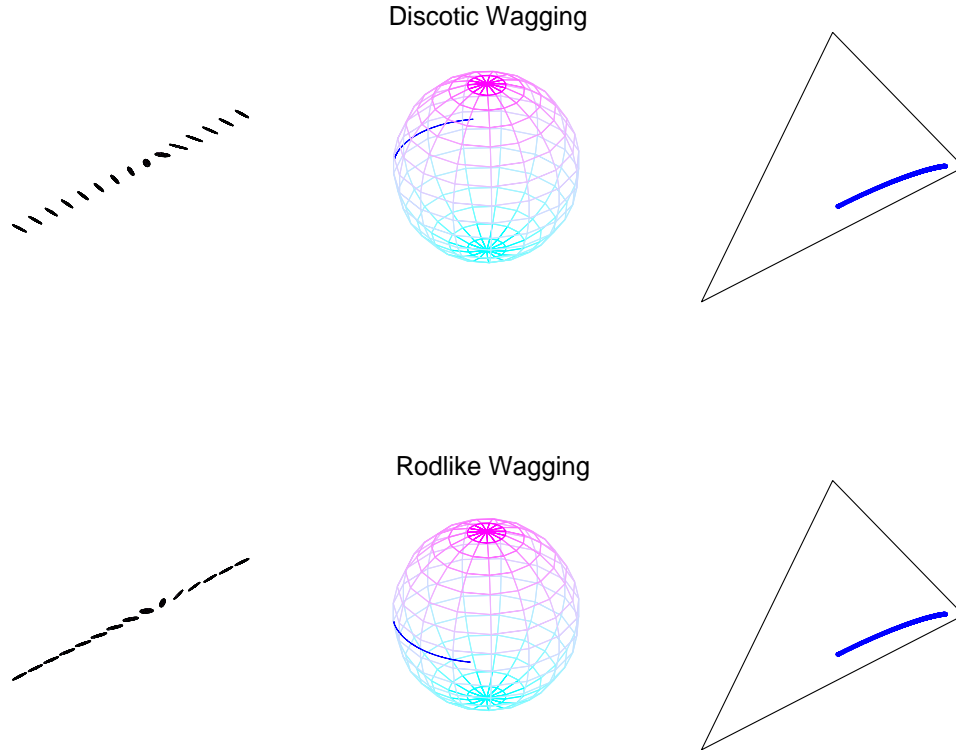


Figure 5: Illustration of the rod-discotic correspondence. The symmetry between rodlike ($a = 0.8$) and discotic ($a = -0.8$) aspect ratios is shown from the modified Doi model with the stable wagging solution at $N = 6, Pe = 2.17$. Note the order parameters are invariant in this symmetry whereas the directors are related by a 90° rotation in the shearing plane. This particular attracting motion occurs right after the tumbling-to-wagging transition, and is clearly associated with significant order parameter variation. This behavior is suppressed in Leslie-Ericksen theory, yet it occurs even for in-plane, wagging motion.

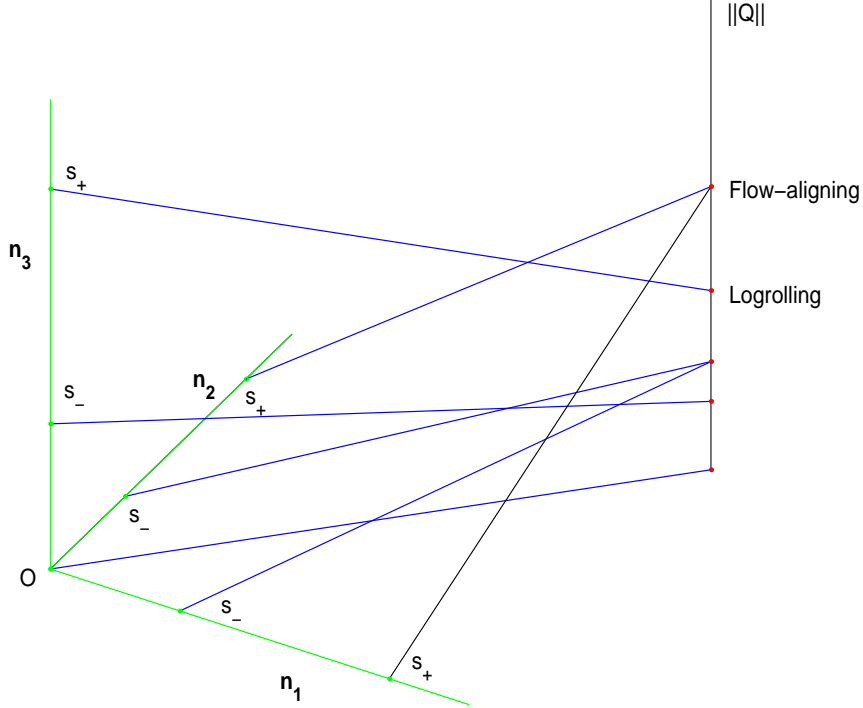


Figure 6: A schematic of the seven solutions (one stable shown in black, six unstable shown in blue) selected in the weak flow limit for the modified Doi model with constant rotary diffusivity, nematic concentration $N = 6$, for infinite aspect ratios ($|a| = 1$). Refer to Figure 2a: for $|a| = 1$ all seven quiescent equilibria lie within the steady region. The isotropic state continues as a nearly isotropic, unstable steady state. Each nematic equilibrium, s_+ and s_- , survives with three steady states emerging from each: two in-plane, flow-aligned **FA** states and one vorticity-aligned, logrolling **LR** state. The in-plane major directors $\mathbf{n}_{1,2}$ are schematic; we do not indicate the different alignment angles for s_+ and s_- . Note s_- is negative, but we depict $|s_-|$ on the schematic. The seven states selected in the weak shear limit are assigned values on a vertical axis labelled by $\|\mathbf{Q}\|$. We use a special norm which distinguishes **FA** vs. **LR** alignment for the same order parameter values, namely, we define $\|\mathbf{Q}\| = Q_{xx}^2 + Q_{xy}^2 + Q_{xz}^2 + Q_{yy}^2 + Q_{yz}^2$.

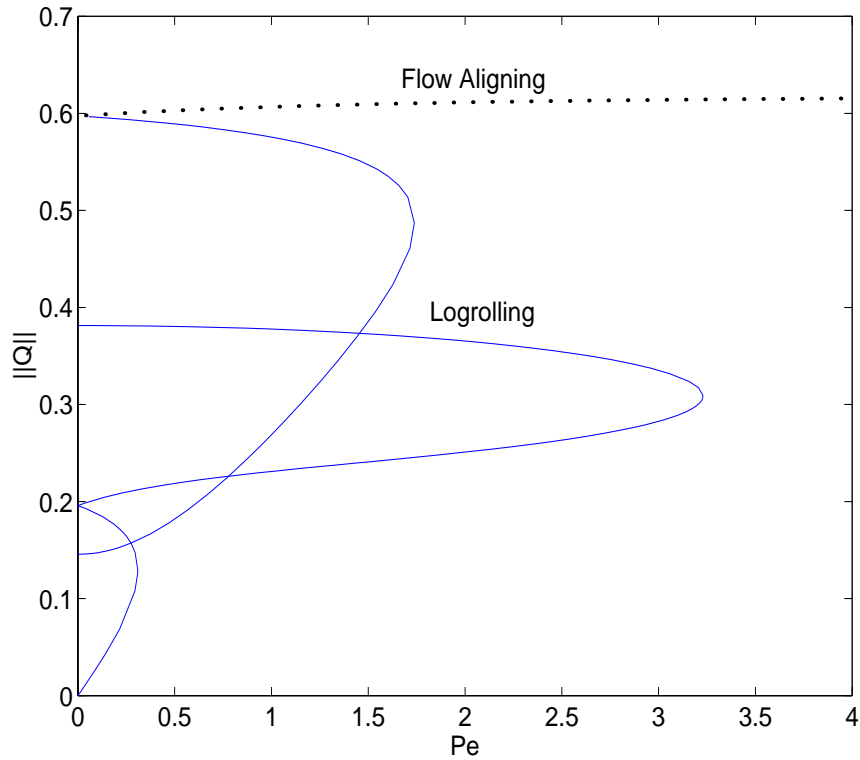


Figure 7: The flow-phase bifurcation diagram of the modified Doi model with constant diffusivity, nematic concentration $N = 6$, and discotic aspect ratio $r^2 = \frac{1}{8}$, or $a = -\frac{15}{17}$, for normalized shear rates $0 \leq Pe \leq 4$. The top dotted (black) curve is the unique stable state, an in-plane, flow-aligning attractor. Six additional solid (blue) curves emerge from the weak shear axis, $Pe \approx 0$, all corresponding to unstable steady states. Referring to Figure 2a, the steady region for this aspect ratio consumes all seven asterisks.

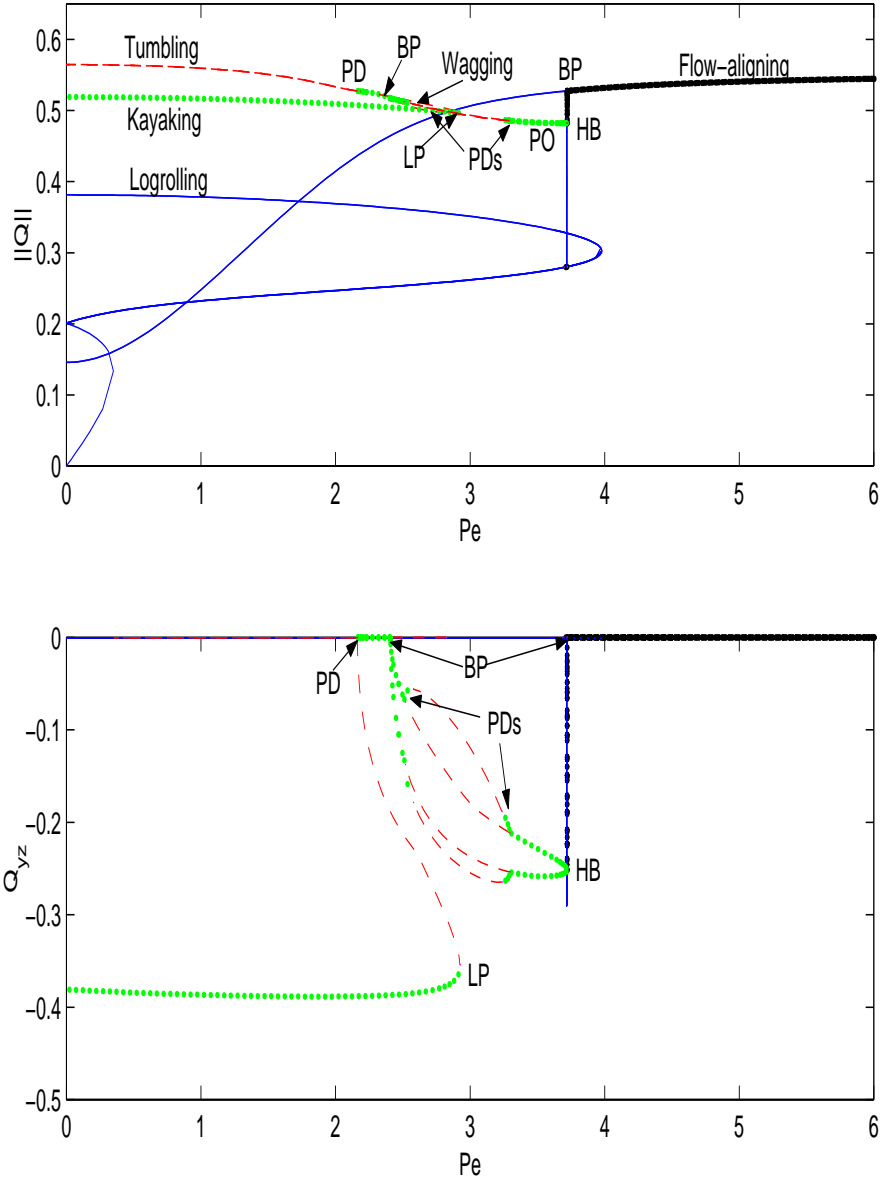


Figure 8: The flow-phase bifurcation diagram for the modified Doi model with constant rotary diffusivity, nematic concentration $N = 6$, and discotic ratio $r = \frac{1}{3}$, or $a = -0.8$. All phase transitions occur within the normalized shear rates $0 \leq Pe \leq 6$, beyond which the unique attractor is an in-plane flow-aligned state. *Black and green branches are stable; blue and red branches are unstable.* The bottom graph is the out-of-plane component Q_{yz} , whose non-zero values distinguish out-of-plane solutions. Between the two pitchfork bifurcations BP that mark in-plane to out-of-plane transitions at $Pe \approx 2.4$ and 3.7 , we give both the maximum and minimum values of Q_{yz} ; these data confirm out-of-plane solutions never cross the shearing plane. The bifurcation labels from XPPAUT are: PD for period-doubling, HB for Hopf, BP for a pitchfork, and LP for a saddle-node bifurcation of out-of-plane periodic states. A cascade of PD bifurcations leading into and out of a window of chaotic attractors for $2.92 < Pe < 3.25$ is not resolved.

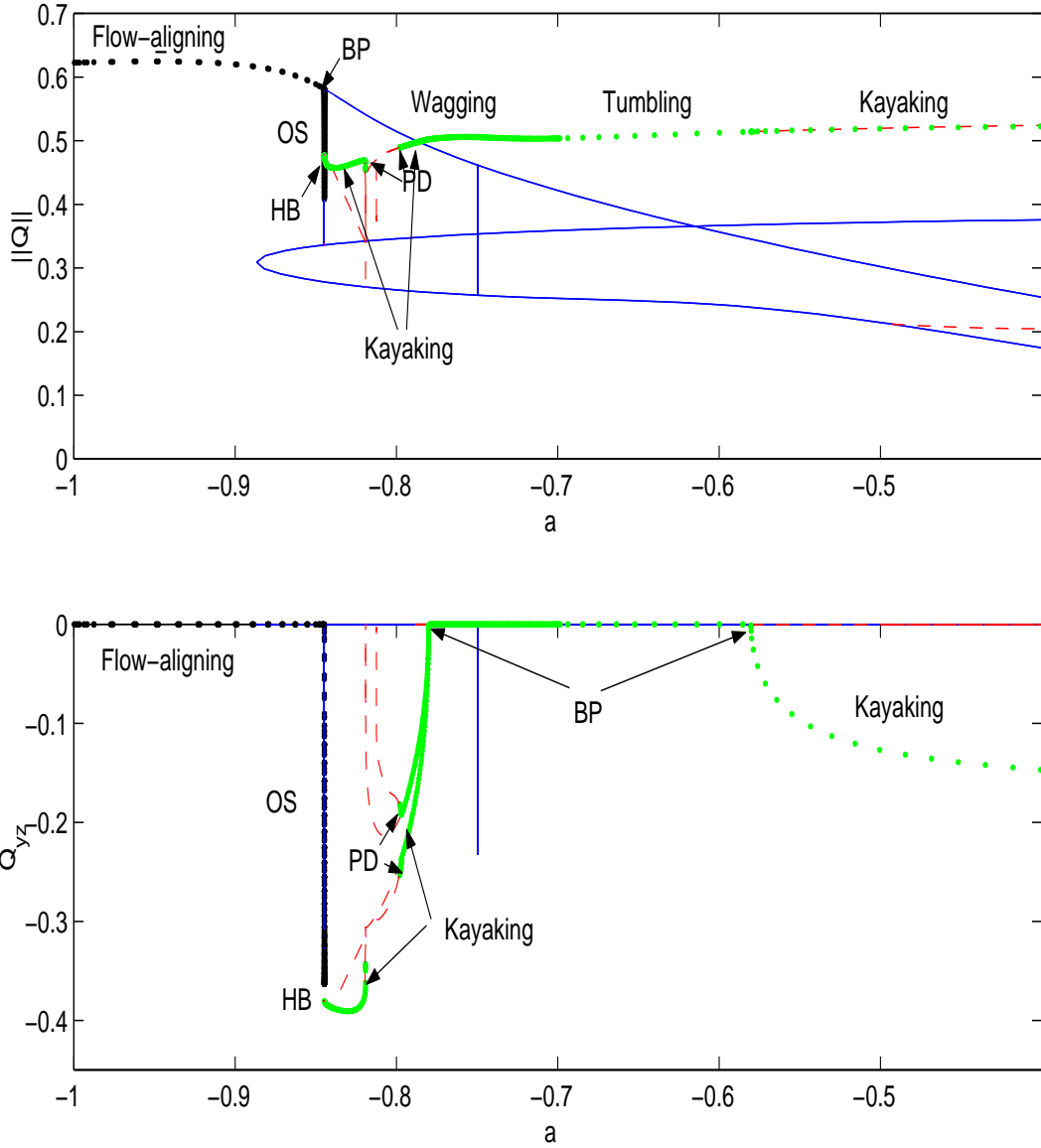


Figure 9: "Virtual bifurcations" of the modified Doi model due to changes in the molecular aspect ratio parameter a , for fixed nematic concentration $N = 6$ and fixed shear rate $Pe = 3.2$. At large enough Pe and extreme aspect ratios $|a| \approx 1$, the only solution is the stable flow-aligning state; Figure 7 illustrates this fact. Here we see a complex bifurcation from a single steady, flow-aligned state at large aspect ratios, to multiple steady/unsteady and in-plane/out-of-plane solution branches, all due to changes in molecular aspect ratio! Critical monodomain phase transitions at specific aspect ratios are predicted: flow-alignment-to-kayaking, kayaking-to-wagging, wagging-to-tumbling, tumbling-to-kayaking, and a period-doubling route to chaotic attractors in the discotic aspect ratio parameter range $-0.8195 < a < -0.7972$.

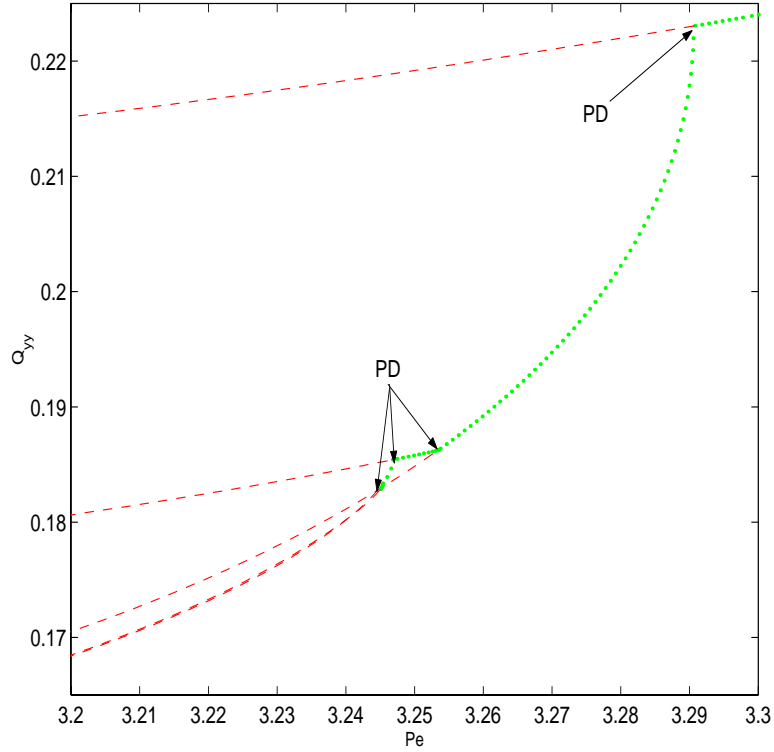


Figure 10: A blow-up of the sequence of period doubling (PD) bifurcations indicated in Figure 8 for the modified Doi model with constant diffusivity, $N = 6$, aspect ratio $r = \frac{1}{3}$, in the normalized shear rate range $3.2 \leq Pe \leq 3.3$. The in-plane component Q_{yy} is used to illustrate the bifurcation structure, entering into the chaotic shear rate range from above. Here we show four PD bifurcations at $Pe \approx 3.29, 3.253, 3.247$ and 3.245 . A PD cascade to chaotic motion occurs rapidly, prior to the value $Pe = 3.24$, which requires a sequence of blowing-up operations to resolve.

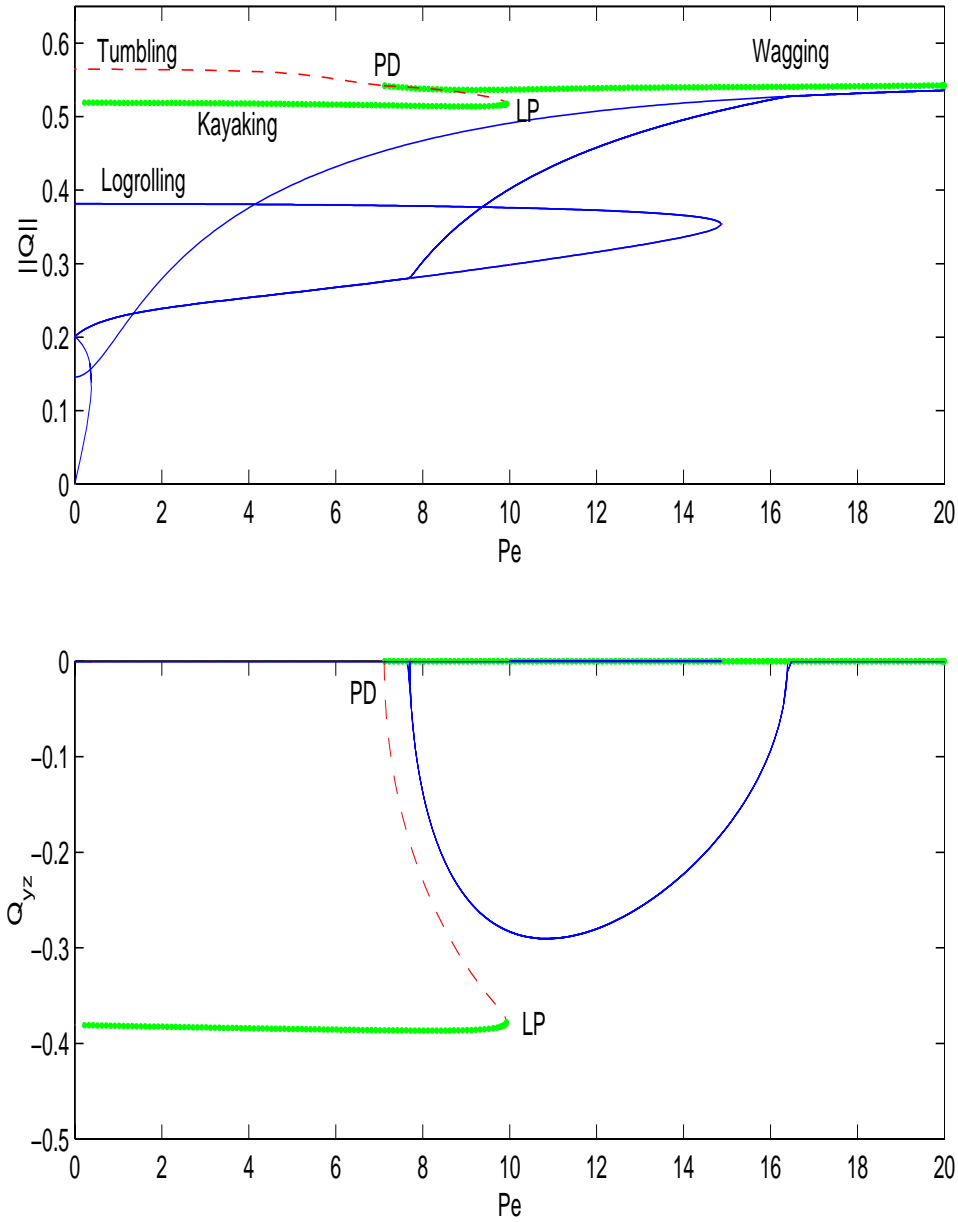


Figure 11: The flow-phase bifurcation diagram of the modified Doi model with orientation-dependent rotary diffusivity and discotic aspect ratio $r = \frac{1}{3}$ (or rod-like ratio 3). The nematic concentration is $N = 6$; all transitions occur within the normalized shear range $Pe \in (0, 20)$. The weak-flow limit analysis, cf. Figure 2a, is independent of diffusivity form, and the flow-selection criteria are identical to Figure 8. The finite-flow bifurcations, however, are clearly modified. The fundamental feature is that the \mathbf{T}/\mathbf{W} branch avoids the sequence of bifurcations of Figure 8, so that the out-of-plane transition to the \mathbf{K}_2 mode, and the subsequent cascade of PD bifurcations with a chaotic attractor, do not occur with orientation-dependent diffusivity in the Doi closure. A wagging to flow-alignment transition occurs for high $Pe > 20$.

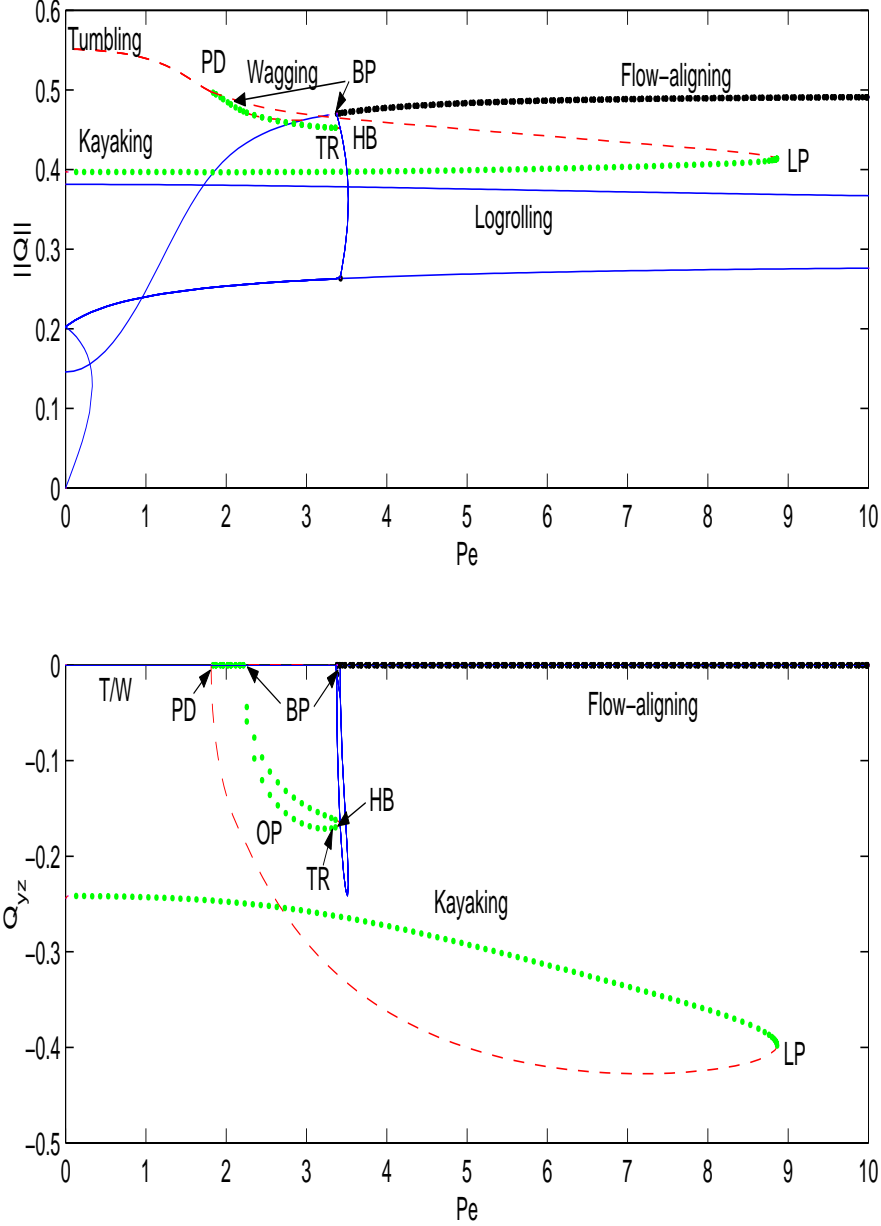


Figure 12: The flow-phase bifurcation diagram for the Rey-Tsuji model with constant diffusivity, nematic concentration $N = 6$, and discotic aspect ratio $r = \frac{1}{3}$, or $a = -0.8$. The flow-induced transitions occur within the normalized shear range $Pe \in (0, 10)$. As noted from Figure 2b together with our analysis of the unsteady selection criteria, the same seven states emerge for the Rey-Tsuji and Doi closures at this aspect ratio. For finite shear rates, the difference between closures lies in the bifurcations of the double branch of \mathbf{K}_2 kayaking modes, each tilted to one side of the shearing plane. In the Rey-Tsuji model, these branches are born in the same way through an out-of-plane instability of a stable wagging mode, but do not undergo a PD cascade to chaos; rather they simply persist until a so-called torus bifurcation (denoted TR by the software XPPAUT) and transition to the stable flow-aligning, in-plane state at $Pe \approx 3.375$. The tumbling to wagging transition takes place roughly at $Pe = 1.79625$, so the stable interval of this branch always consists of wagging motion.

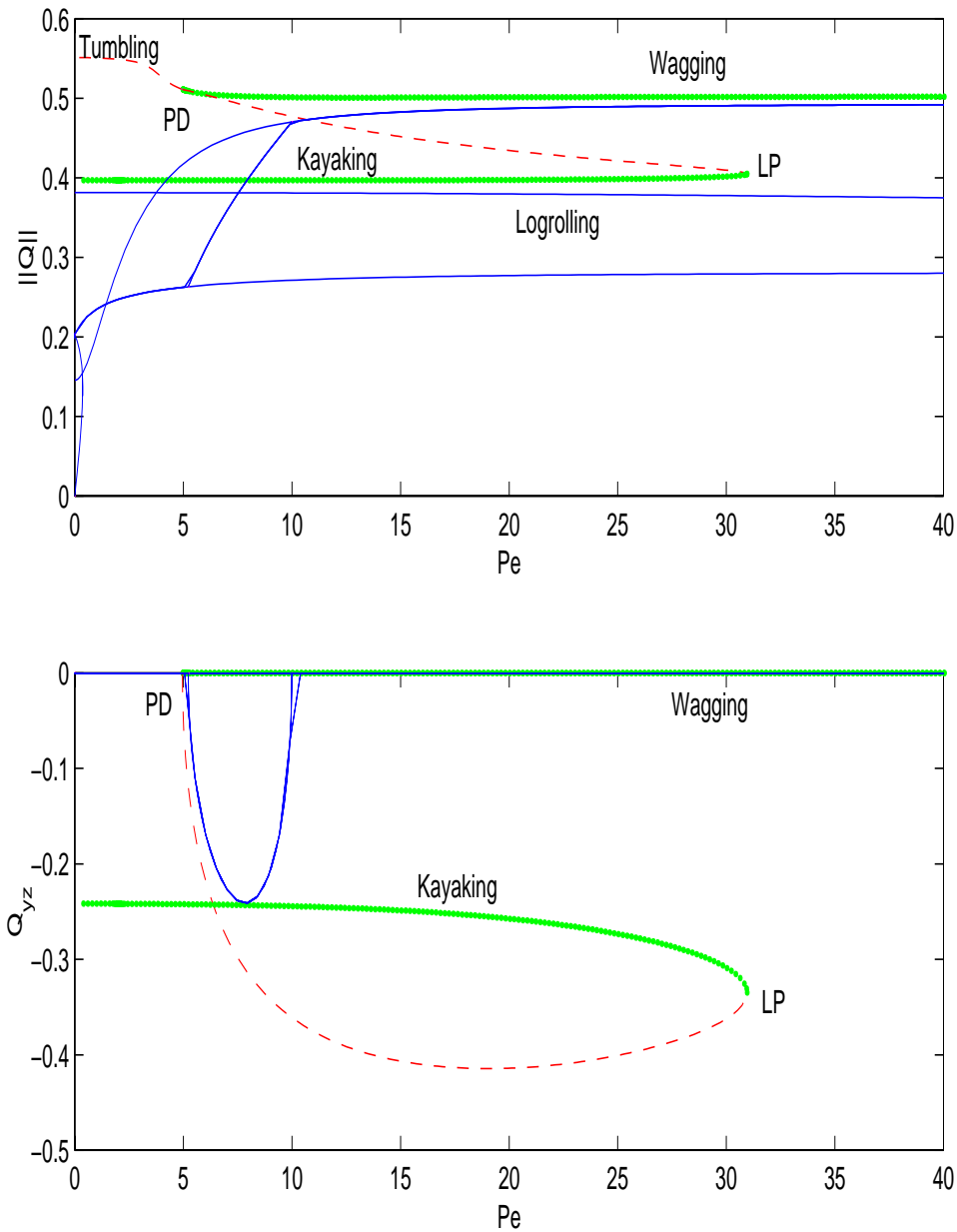


Figure 13: The flow-phase bifurcation diagram for the Doi-Rey-Tsuji model with orientation-dependent rotary diffusivity, $N = 6, a = -0.8$. The bifurcations are similar to those of previous diagrams. Two primary stable branches emerge over this range of Pe , overlapping for an interval of Pe leading to bi-stable attractors. The tumbling-wagging transition takes place at $Pe = 5.834$.

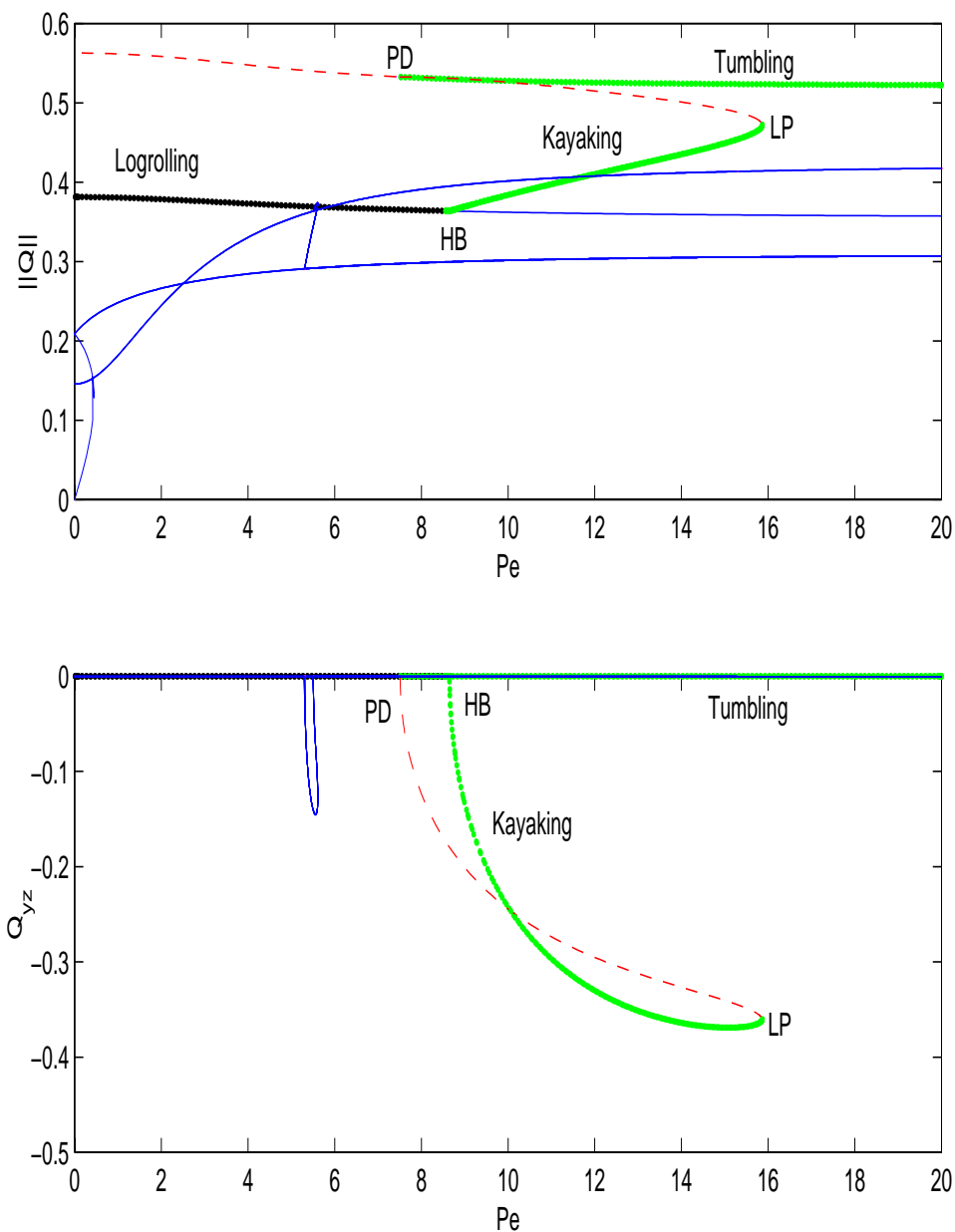


Figure 14: The bifurcation diagram for the Doi-HL1 model with constant diffusivity, $N = 6$, and shape parameter $a = -\frac{24}{26}$ corresponding to discotic aspect ratio $r = \frac{1}{5}$. As explained in Figure 2c and surrounding text, this closure selects a *unique, stable* \mathbf{LR} steady state in weak shear. This stable branch persists until a Hopf bifurcation at $Pe \approx 8.638$ creates a stable \mathbf{K}_1 kayaking branch, in which the major director now rotates around the vorticity axis. The stable kayaking branch persists until a saddle-node bifurcation at $Pe \approx 15.85$. (A physically inconsequential bifurcation occurs for Pe between 5 and 6, leading to unstable kayaking solutions.) The unstable \mathbf{T} solution arising from s_+ in weak shear stabilizes at $Pe \approx 7.509$ through a PD bifurcation, remaining stable beyond $Pe = 20$. The stable attractors are summarized in Table 5.

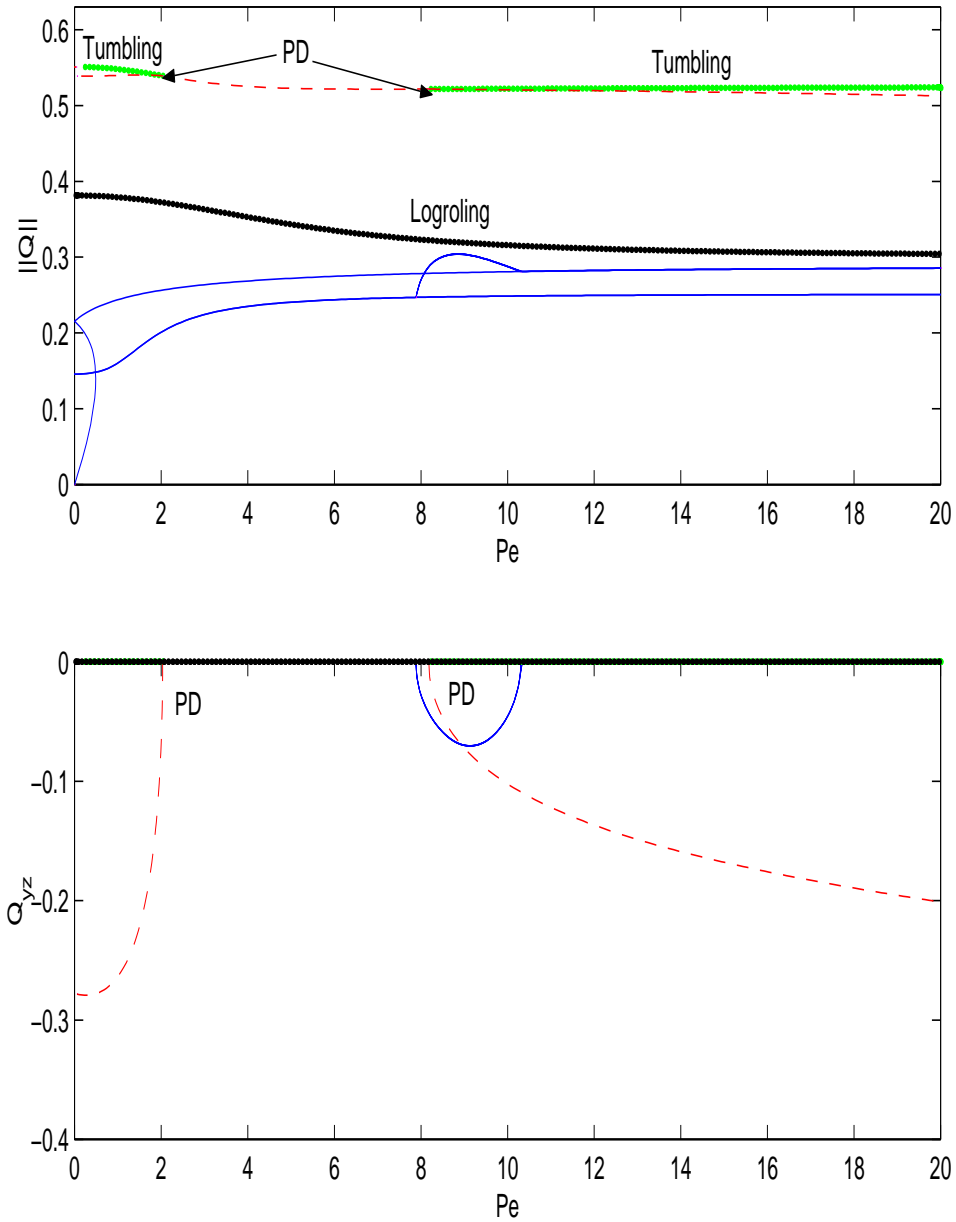


Figure 15: The bifurcation diagram for the Doi-HL2 model. The parameter values are $N = 6, a = -\frac{24}{26}$. The logrolling steady state exists for all values of Pe and is stable. Tumbling/wagging stable solutions exist at low and high shear rates, first losing stability in a PD bifurcation at $Pe = 2.034$, then regaining stability in another PD bifurcation at $Pe = 8.179$.